OPEN ACCESS
Functional Materials Letters
Vol. 15, No. 5 (2022) 2240001 (26 pages)

DOI: 10.1142/S179360472240001X

World Scientific
www.worldscientific.com

Lithium phosphosulfide electrolytes for solid-state batteries: Part I

Xin Lu[*,†,**], Chih-Long Tsai[*], Shicheng Yu[*], Hongying He[‡], Osmane Camara[*], Hermann Tempel[*], Zigeng Liu[*], Anna Windmüller[*], Evgeny V. Alekseev[*], Shibabrata Basak[*,§], Li Lu[¶], Rüdiger-A. Eichel[*,†] and Hans Kungl[‖]

[*]*Institut für Energie-und Klimaforschung (IEK-9: Grundlagen der Elektrochemie) Forschungszentrum Jülich, D-52425 Jülich, Germany*

[†]*Institut für Materialien und Prozesse für elektrochemische Energiespeicher-und wandler RWTH Aachen University, D-52074 Aachen, Germany*

[‡]*School of Mechanical and Aerospace Engineering, Nanyang Technological University Singapore 639798, Singapore*

[§]*Ernst Ruska-Centre for Microscopy and Spectroscopy with Electrons and Peter Grünberg Institut Forschungszentrum Jülich, D-52425 Jülich, Germany*

[¶]*Department of Mechanical Engineering, National University of Singapore Singapore 117575, Singapore*

[‖]*Institut für Energie-und Klimaforschung (IEK-12: Helmholtz-Institute Münster Ionics in Energy Storage), Forschungszentrum Jülich, D-48149 Münster, Germany*

[**]*x.lu@fz-juelich.de*

Received 31 May 2022; Accepted 1 July 2022; Published 31 August 2022

A high performance and stable Li-ion conductive solid electrolyte is one of the key components for the future all-solid-state batteries with metallic lithium anodes. Phosphate, oxide and phosphosulfide-based inorganic solid electrolytes are currently under development. High ambient temperature Li-ion conductivities amounting up to 10^{-2} S cm^{-1} for the best performing electrolytes distinguish the phosphosulfides from the other material systems. Part I of the review starts with the motivation and background for the development of Li-phosphosulfide electrolytes followed by an overview of four different types of phosphosulfide electrolytes; the Li–P–S, thio-LiSICon, LGPS and the Argyrodite-type electrolytes. The core of part I is concerned with a detailed discussion of the phosphosulfide electrolyte types that have been under investigation already for a long time, the Li–P–S and the LiSICon. There is a multiplicity of different compositions within each of these types. The idea behind the outline of these sections is to point out the relations and differences between the different materials with respect to their chemistry related to the phase diagrams. Patterns for the relations among the materials identified in the phase diagrams are the base for a discussion of structure, processing and Li-ion conductivity within separate sections for each type and resulting in intra-type comparisons. The follow up part II will continue with a treatment of the more recently developed LGPS and Argyrodite-type electrolytes tracking the same concept, before addressing an inter-type comparison of ambient temperature Li-ion conductivities and the electrochemical stability of the electrolytes *vs.* metallic lithium. A final section in part II summarizes conclusions and provides perspectives for future research on Li-ion conductive phosphosulfide electrolytes.

Keywords: Lithium sulfide; thio-LiSICon; sulfide electrolytes; solid-state electrolytes.

1. Introduction

In the past few decades, the use of lithium-ion batteries (LIBs) has become prevalent in our day-to-day lives. These batteries have been the leaders in the market ever since they were first commercialized in 1991 by Sony and Asahi Kasei.[1] From portable devices such as laptops and smartphones to large electrical vehicles, LIBs are the preferred energy storage systems over other energy storage devices due to their long-term cycle life and high energy densities compared with other energy

[**]Corresponding author.

storage systems. However, due to the ever increasing need for higher energy density and cycle life, the development of newer battery technology is crucial.[2]

The main motivation for the development of batteries with solid-state electrolytes is to obtain higher specific energies and energy densities in future batteries. On the cell level, the use of low volume and low weight Li-metal anodes is the main source for the intended improvement. In addition, volume reduction may result from thinning the electrolyte layer compared to those required in batteries with liquid electrolyte. However, this advantage is counteracted by the requirement of considerable fractions of solid-state electrolyte in the cathode in order to ensure the Li-transport within the electrode. Despite these considerations, reductions of volume and weight are expected on the package level.

Safety concerns and the design of solid-state batteries are closely related. While the batteries with graphite-based anodes seemed to have overcome the safety issues resulting from dendrite growth and overheating, the concerns of safety become a paramount point when using Li-metal anodes. Thus, solid-state electrolytes have, beside the need for high Li-ion conductivity, to fulfill the requirements such as electrochemical stability *vs.* metallic lithium and resistivity against dendrite growth that emerge from design concepts underlying the all-solid-state battery using an Li-metal anode.

To address these issues and challenges for solid-state electrolytes, a lot of research work has been focused on oxide- and phosphate-based Li-ion conductors with Ta or Al-doped lithium-lanthanum-zirconates ($Li_{7-x}La_3Zr_{2-x}Ta_xO_{12}$ and $Li_{7-3x}Al_xLa_3Zr_2O_{12}$) and LiSICon (lithium superionic conductors)-based oxides such as lithium-phosphorus oxide and lithium-germanium-zinc oxide (Li_3PO_4 and $Li_{2+2x}Zn_{1-x}Ge_xO_4$) being the most prominent materials for the first, and lithium-aluminum-titanium phosphate ($Li_{1+x}Al_xTi_{2-x}(PO_4)_3$ LATP) being representative for the second class of materials. These electrolytes have been intensively studied due to their relative ease of handling.

Although there were early developments for sulfurbased electrolytes since the late 1980s, when Ahn and Huggins reported the Li-ion conductivity in Li_4SiS_4,[3] the big push for researching sulfur and phosphosulfide electrolytes started with the work of Kanno and his group around the millennium.[4,5]

Based upon the evaluation of isostructural materials that are equal with respect to their cationic components, but different (comparing oxygen *vs.* sulfur) regarding the anodic component, they promoted the idea and the concept of high-polarizing polyanions with sulfur to be favorable to enhanced Li-ion conduction (Fig. 1).

Since then, there has been growing interest in lithium phosphosulfide electrolyte materials. Initial work was concerned with the Li–P–S type (Li_7PS_6, Li_3PS_4 and $Li_7P_3S_{11}$) and thio-LiSICon type materials. In particular, with respect to the former system, researches on glass and glass ceramic electrolytes were developed in parallel to the investigations on the crystalline materials. Other than the Li–P–S system, Deiseroth *et al.* in 2008 discovered Li-ion conductors with a halogen substituted Argyrodite-type phosphosulfide electrolyte, which showed high Li^+ ion mobility by utilizing the Argyrodite structure.[6] A breakthrough was achieved in 2011 by Kamaya *et al.* with the synthesis of $Li_{10}GeP_2S_{12}$, commonly referred to as LGPS, which created a hype in the scientific community due to its high ambient temperature Li-ion conductivity of 10^{-2} S cm^{-1}.[7] In spite of the demanding requirements for the preparation of the phosphosulfide materials, search for an Li-ion conducting electrolyte fulfilling all

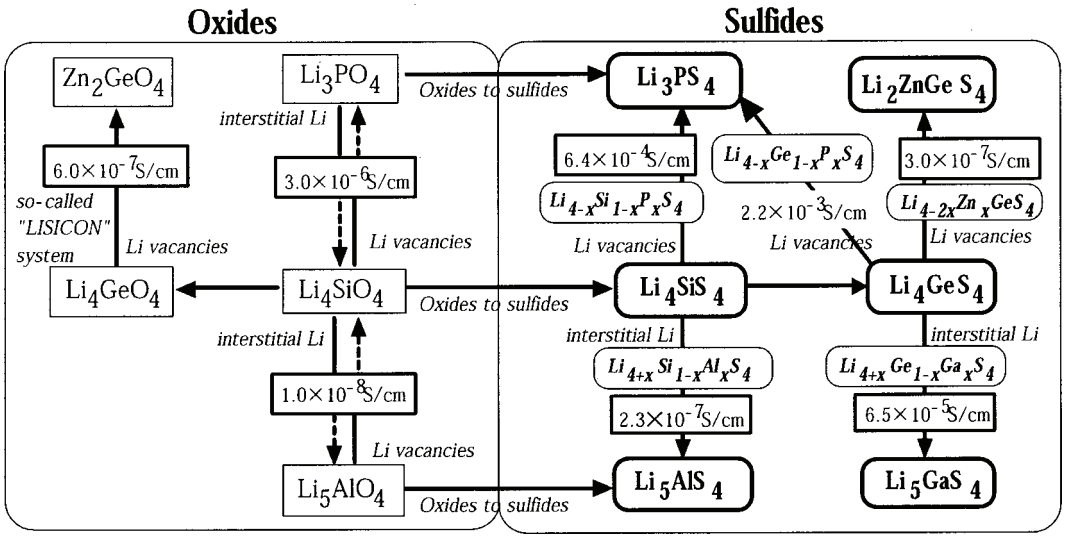

Fig. 1. The concept of material design for the thio-LiSICon system. Reprinted with permission from Kanno *et al.* © 2001 ECS — The Electrochemical Society.[4]

the necessary criteria for application in an all-solid-state battery was intensified around the world.

There are several excellent reviews on the topic, some give a compound analysis of all the issues that are related to the phosphosulfide electrolyte applications, while others are focused on specific aspects or limit analysis to a specific type of phosphosulfide electrolyte.[8–16] In particular, the relations between structure and conductivity, liquid phase processing, stability towards humid air and interfaces have been discussed intensively.

In part I of the review, the motivation for the development of the phosphosulfide electrolytes is pointed out in a brief introduction, followed by an overview over the four major types of phosphosulfide electrolytes, the Li–P–S, thio-LiSICon, LGPS and the Argyrodite type. Subject to detailed discussions in part I will be the relations between chemistry and phase diagrams, the structure, the processing and the conductivity for the Li–P–S and the thio-LiSICon type electrolytes. Focus is put on discussion of the chemistry related to the phase diagrams and the Li-ion conductivities at ambient temperature, while some background information is presented on structure and processing. Part II of the review then starts with the discussion of these four issues for LGPS and Argyrodite-type electrolytes, before turning to summarizing sections comparing representative electrolytes for all the four types with respect to the conductivity and electrochemical stability *vs.* metallic lithium. Part II will be concluded with remarks on status and perspectives for the development of phosphosulfide electrolytes.

2. Types of Crystalline Phosphosulfide Electrolyte Materials

Crystalline lithium phosphosulfide Li-ion conductors can be categorized into the four groups denoted as Li–P–S type, thio-LiSICon, LGPS-type and Argyrodite-type materials. The Li–P–S type electrolytes are distinguished from the other materials in that they contain exclusively lithium, sulfur and phosphorus as elements. According to their components, they can also be labeled as $Li_xP_yS_z$ type electrolytes.

Characteristic for both, thio-LiSICon and LGPS-type electrolytes, is the arrangement of all the sulfur in the material in the form of PS_4^{3-} or MS_4^{2-}, MS_4^{3-} or MS_4^{-} polyanions, such that no free sulfur anions or phosphate complexes other than the aforementioned are present in the material. With respect to their chemistry, these materials mostly contain a metal or a semi-metal element. The distinction between the thio-LiSICon and the LGPS type is related to their structures. The term LGPS-type electrolytes, where LGPS stands for $Li_{10}GeP_2S_{12}$, the prototype electrolyte of this group, is exclusively used for the phosphosulfides with tetragonal space group $P4_2/nmc$. $Li_{10}GeP_2S_{12}$ was the first solid-state electrolyte with Li-ion conductivity higher than 10^{-2} S cm^{-1} at ambient temperature.[7]

Historical development of the thio-LiSICon emerged from the corresponding isostructural oxide systems labeled (oxide-) LiSICons. Originally, materials with structure equal or similar to orthorhombic γ-Li_3PS_4 or orthorhombic β-Li_3PS_4 were attributed to the thio-LiSICon type. Along with the extensive developments of new compositions, the term LiSICon type was extended to sulfide and phosphosulfide materials with lower symmetry such as monoclinic-structured materials.[17] Considering the chemical composition of thio-LiSICon, there are several characteristic stoichiometries with Li_4MS_4 and $Li_{4-x}M'_{1-y}M''_yS_4$ being most prominent compositions among them.[7]

Argyrodite electrolytes are defined by the cubic space group $F43m$. They are named according to the structure of the mineral Argyrodite Ag_8GeS_6.[18] Typically, at least so far in contrast to most other phosphosulfide electrolyte types, Argyrodites contain halogen elements as a component. However, there are also halogenfree semi-metals containing Argyrodite compositions.

Among the Li–P–S type electrolytes, the Li_2S:P_2S_5 materials span a relatively wide range of Li_2S:P_2S_5 ratios with a minimum Li_2S content of 50 mol.% and a maximum Li_2S content of 87.5% on the corresponding tie line on the left hand of the phase diagram (blue shaded area). Modifications in Li-content of the Li_2S:P_2S_5 base materials can be displayed by setting Z = Li. Considering the thio-LiSICon system, Z is identified with a (semi) metal-disulfide $Z = MS_2$. Contents of 20–30% metal- and/or semi-metal-disulfides and P_2S_5 contents below 10% are typical for the Li-ion conductors of the thio-LiSICon type (yellow shaded area). Phosphorous-free materials in this system Li_4MS_4 are displayed on the tie line Li_2S–Z in such type of phase diagram.

In contrast, relatively low contents of metal- or semi-metal-disulfides (< 20%) along with high Li_2S contents, almost comparable to those of the upper values of the Li_2S:P_2S_5 system, are characteristic for the LGPS-type materials (red shaded area). With corresponding Z components, the LGPS materials are on or close to the tie line between Li_3PS_4 and phosphorusfree thio-LiSICon Li_4MS_4.

With respect to their chemistry, fundamentally different electrolyte materials exist within the Argyrodite system (green shaded area). On the one hand, Argyrodites containing halogens (Z = LiX with X = Br, Cl or I) have Li_2S around 60%, markedly lower than that of LGPS. In the phase diagram, the halogen-type Argyrodite electrolytes show up on the tie line $Li_{10}P_2S_{10}$–LiX. On the other hand, Argyrodite electrolytes with semi/metal components have an even lower Li_2S content of 50%.

A ternary phase diagram with components Li_2S–P_2S_5–Z (Fig. 2), in which Z has to be interpreted with respect to the

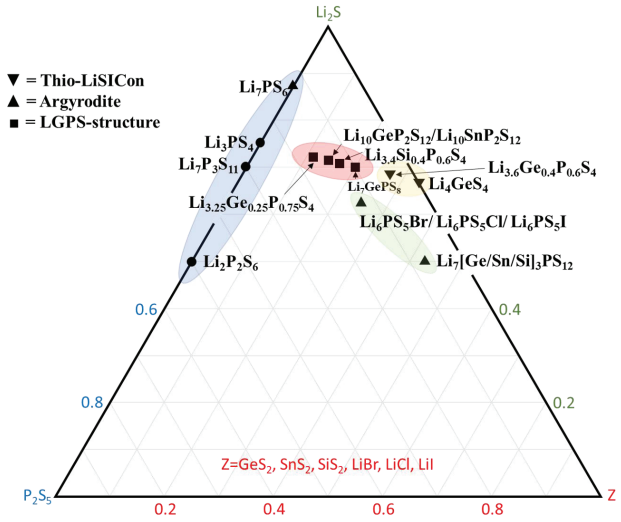

Fig. 2. Lithium phosphosulfide systems displayed in a ternary Li_2S–P_2S_5–Z phase diagram. Blue area denotes $Li_xP_yS_z$, red is for LGPS-type materials, yellow corresponds to the $Li_{4-y}M'_{1-y}M''_yS_4$ type and green is for Argyrodites. Z may stand either for a metal or semi-metalsulfur compound or a lithium-halogenide. Scales are in mol.%.

elements in the systems under consideration, provides an overview about the relative amounts of components Li_2S and P_2S_5 along with varying Z. Moreover, it may give a first impression on the amounts of components with cationic and anionic ($P_xS_y^{z-}$) characteristics. However, care has to be taken when evaluating the anionic and cationic characteristics for the materials according to this type of diagram. First, the phosphorus–sulfur polyanions can be present in various forms and different formal charges. *Ortho*-thiophosphate PS_4^{3-}, *pyro*-thiophosphate $P_2S_7^{4-}$ and *meta*-thiodiophosphate $P_2S_6^{2-}$ moieties and S^{2-} are the most typical anionic species in Li_2S–P_2S_5 type electrolytes. Second, in addition to the anionic characteristic of these species, additional influence from the "third" component Z requires detailed analysis. GeS_4^{2-} tetrahedra are present in thio-LiSICon and LGPS-type materials.[19] In oxygen-substituted LGPS and halogen-containing Argyrodites, there are substantial contributions to the anionic characteristics from these components. Thus, with respect to polarizability, the overall phase diagram can provide only limited information, in particular when comparing materials for which Z is different.

3. Li–P–S Type Electrolyte Materials

Li–P–S type Li-ion conducting materials encompass the most important base compositions $Li_2P_2S_6$, $Li_7P_3S_{11}$, Li_3PS_4, and Li_7PS_6 electrolytes. A major role in the development of these materials was played by investigations of glass ceramic materials, in particular Li_3PS_4 and Li_7PS_6. Previous research on isostructural materials such as Li_3PO_4 (the oxide of LiSICon) and Argyrodites promoted the elaboration of this

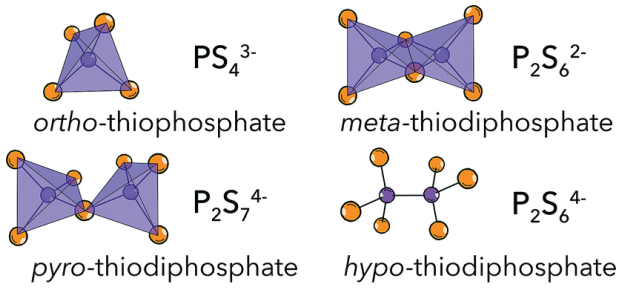

Fig. 3. Phosphorus–sulfur anionic species in Li–P–S type electrolytes. Reproduced from[10] with permission from the Royal Society of Chemistry.

type of crystalline electrolytes.[20,21] All these base materials can be considered as rooted in Li_2S and P_2S_5. The compositions with respect to the Li_2S:P_2S_5 ratios are 50:50, 70:30, 75:25 and 87.5:12.5 for $Li_2P_2S_6$, $Li_7P_3S_{11}$, Li_3PS_4, and Li_7PS_6, respectively.

Characteristic for these materials is the (poly-) anion building blocks, which are formed in an interplay of sterical conditions and composition while also being major determinants of the structure. *Ortho*-thiophosphate PS_4^{3-}, *pyro*-thiophosphate $P_2S_7^{4-}$ and *meta*-thiodiphosphate $P_2S_6^{2-}$ moieties and S^{2-} are the most important building blocks of the anion lattice structures in electrolytes with pentavalent phosphorus. Lower relative Li_2S content favors the formation of the *meta*- and *pyro*-thiophosphate phosphorus–sulfur polyanions, whereas at high relative fractions, the materials of the polyanions tend to be present in the form of *ortho*-thiophosphate and in part in the form of S^{2-} (Fig. 3).[12]

Modifications of the compositions cover not only materials that can be regarded as Li_2S–P_2S_5 mixtures but also materials whose composition does not correspond to any Li_2S–P_2S_5 ratio. Most important for the former type is a series of $Li_{3+5x}P_{1-x}S_4$ electrolytes.[22] The second type of non Li_2S–P_2S_5 compositions encompass $Li_4P_2S_6$,[23,24] $Li_{3-x}PS_4$,[25] Li_3PS_{4+n},[26] and most importantly, the $Li_{9.6}P_3S_{12}$ high conductivity electrolyte discovered by Kato *et al.*[27]

3.1. *Chemistry and phase relations of Li–P–S type electrolytes*

Considering the chemical composition, the ternary phase diagram Li–P–S reveals the elemental fractions in the materials and the P:S ratios of the materials, which indicate the conditions for the phosphorus–sulfur tetrahedra formation from a stoichiometric point of view. All the base materials $Li_2P_2S_6$, $Li_7P_3S_{11}$, Li_3PS_4, and Li_7PS_6 lie on a tie line connecting Li_2S–P_2S_5 with Li-content being lowest for $Li_2P_2S_6$ and highest for Li_7PS_6 (Fig. 4(a)).

The conditions for the formation of phosphorus–sulfur polyanions from the chemical point of view can be related to the intersection points of the tie lines between Li and the respective

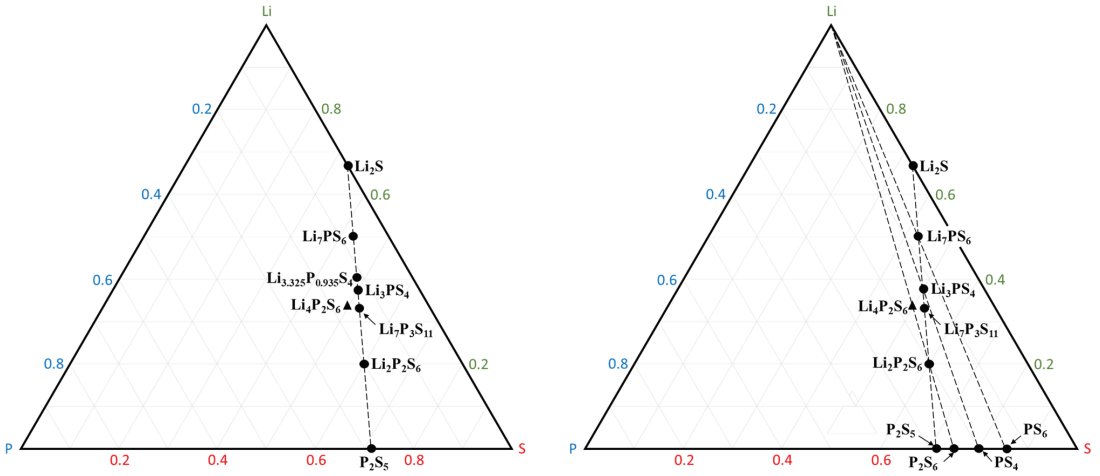

Fig. 4. Ternary phase diagram Li–P–S (a) with representation of the positions for $Li_xP_yS_z$ materials. (b) Including tie lines defined by Li–$Li_2P_2S_6$, Li–Li_3PS_4 and Li–Li_7PS_6, all of them extended toward the P–S axis. Scales are in mol.%.

composition $Li_xP_yS_x$, extended toward the *P–S* axis, with the *P–S* base tie line in the diagram (Fig. 4(b)). The intersection point gives the P and S fractions (or P:S ratios) for all the compositions along the complete tie line defined by Li and $Li_xP_yS_x$. While the mere figures for the P:S ratios for $Li_2P_2S_6$, $Li_7P_3S_{11}$, Li_3PS_4, and Li_7PS_6, i.e., 75:25, 78.5:21.5, 80:20 and 85.7:14.3 seem not very different, there are substantial consequences with respect to the type of anion moieties that can be formed.

In Li_3PS_4, the P:S ratio matches exactly the 1:4 ratio of these elements required for the formation of *ortho*-thiophosphate PS_4^{3-}. In fact, the anion sublattice is composed exclusively from this type of isolated phosphorus–sulfur tetrahedra. The P:S ratios for $Li_2P_2S_6$ and $Li_7P_3S_{11}$ are lower than 1:4. This immediately implies, that at least not all phosphorus–sulfur polyanions can be isolated tetrahedral PS_4^{3-}, the lack of sulfur in these materials requires the formation of other types like thiodiphosphates *meta-* and *pyro*-thiophosphate, in which part of the sulfur is shared by the two tetrahedral units. In contrast, the P:S ratio for Li_7PS_6 is 1:6, thus arrangement of the phosphorus in this material, even in the form of tetrahedra with the highest possible P:S ratio, i.e., PS_4^{3-} will leave an excess of sulfur. Although from consideration of the phase diagrams it is not possible to give a statement on the actual configuration of the anion types realized in specific materials, they allow to distinguish between combinations that are possible and impossible configurations.

Development on $Li_{3+5x}P_{1-x}S_4$ type modifications of Li_3PS_4 was based on the idea to enhance the lithium content in the base material, while keeping the charges balanced by reducing the phosphorus fraction.[22] The $Li_{3+5x}P_{1-x}S_4$ series was investigated in a range of $0 \le x \le 0.27$, which encompasses materials with compositions of Li_3PS_4, $Li_{3.555}P_{0.888}S_4$, $Li_4P_{0.8}S_4$ and $Li_{4.36}P_{0.73}S_4$ corresponding to Li_2S:P_2S_5 ratios 3:1, 4:1, 5:1 and 6:1, respectively. All compositions to lay on the Li_2S–P_2S_5 tie line positions between Li_3PS_4 and Li_7PS_6 (Fig. 4(a)). The intention for the design of these materials was to enhance the Li-ion conductivity by creating Li-interstitials. However, as a consequence of the P:S relations, there have to be also changes in the anion sublattice due to the lower content in phosphorus when compared to a P:S ratio of 1:4.

The second type of modifications of Li_2S:P_2S_5 type base electrolytes are materials that are not Li_2S–P_2S_5 rooted; i.e., the compositions of these materials cannot be represented in terms of an Li_2S:P_2S_5 ratio. Consequently, the positions of such materials in a ternary Li–P–S diagram are off the Li_2S–P_2S_5 tie line.

Among them is $Li_4P_2S_6$, one of the first crystalline phosphosulfide materials that was successfully synthesized,[23] which is very different from the Li_2S–P_2S_5 type electrolytes. With respect to its stoichiometry, it can be considered either as related to $Li_2P_2S_6$ (Li_2S:P_2S_5 ratio of 50:50) with enhanced Li-content or related to $Li_4P_2S_7$ (Li_2S:P_2S_5 ratio of 67:33) with a reduced sulfur content. Each of these characterizations defines the off-tie line position of $Li_4P_2S_6$ relative to the Li_2S–P_2S_5 type materials (Fig. 4(a)). However, considering the anion lattice type, in $Li_4P_2S_6$, none of the moieties present in the Li_2S–P_2S_5 type electrolytes is realized. Instead, the polyanions are formed as $P_2S_6^{4-}$ hypo-thiodiphosphate moieties. Along with the decrease in the sulfur content *vs.* $Li_4P_2S_7$, the phosphorus in $Li_2P_2S_6$ adopts a P^{4+} formal charge state and a corresponding polyanions formation.

Li_3PS_4 has been used as the base material to synthesize Li-deficient $Li_{3-y}PS_4$ (y = 0.1, 0.15, 0.2 and 0.3) as well as Li-excess $Li_{3+x}PS_4$.[25] In the Li–P–S ternary phase diagram, these materials are on the tie line between Li and PS_4 (Fig. 5). Lithium-deficient materials $Li_{3-y}PS_4$ were prepared in a compositional range y = 0.1, 0.15, 0.2 and 0.3. The highest Li-deficit in these material series results in $Li_{2.7}PS_4$ (Fig. 5).[25]

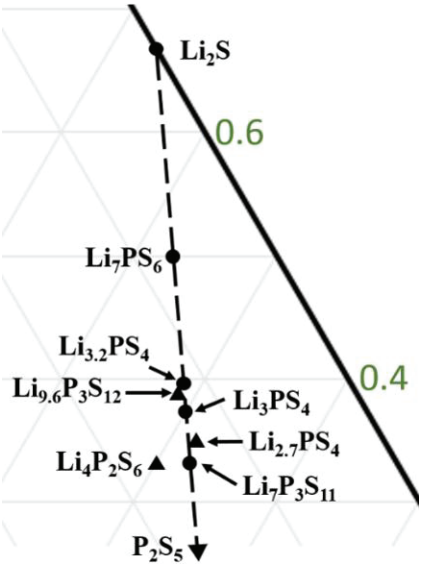

Fig. 5. Tie line between Li_2S–P_2S_5 showing off tie line compounds $Li_{9.6}P_3S_{12}$, $Li_{2.7}PS_4$, $Li_4P_2S_6$.

Most important among the non-Li_2S–P_2S_5 type materials, however, is the high conductivity off-stoichiometric electrolyte $Li_{9.6}P_3S_{12}$ that has been discovered only recently.[27] As the formula given in a form normalized to S_4 indicates a design concept for $Li_{9.6}P_3S_{12}$ = $Li_{3.2}PS_4$ similar to the $Li_{3+5x}P_{1-x}S_4$ series with respect to the Li_3PS_4 base along with an enhanced lithium content.[22] In contrast to the $Li_{3+5x}P_{1-x}S_4$, series, in which the addition of five units of Li^+ goes along with the reduction in one unit of P^{5+}, the $Li_{9.6}P_3S_{12}$ is not balanced with respect to these formal charges on doping Li_3PS_4 with lithium. On the other hand, when compared to the material from the $Li_{3+5x}P_{1-x}S_4$ series with the same Li-content $Li_{3.2}P_{0.96}S_4$ (corresponding to $Li_{3+5x}P_{1-x}S_4$ with $x = 0.04$), $Li_{3.2}PS_4$ can be considered as a phosphorus excess modification of the former material. The difference in phosphorus content implies an impact on the anion sublattice. In the materials of $Li_{3+5x}P_{1-x}S_4$ series, such as $Li_{3.2}P_{0.96}S_4$, the P:S ratio differs from 1:4, whereas in $Li_{9.6}P_3S_{12}$ the ratio exactly matches this ratio required for an exclusive arrangement of the phosphorus and sulfur in the form of *ortho*-thiophosphate PS_4^{3-} (Fig. 5).

3.2. *Li–P–S structure*

$Li_2P_2S_6$ crystallizes in a monoclinic space group *C/m*. The type of thiophosphate building blocks in this material is quasi

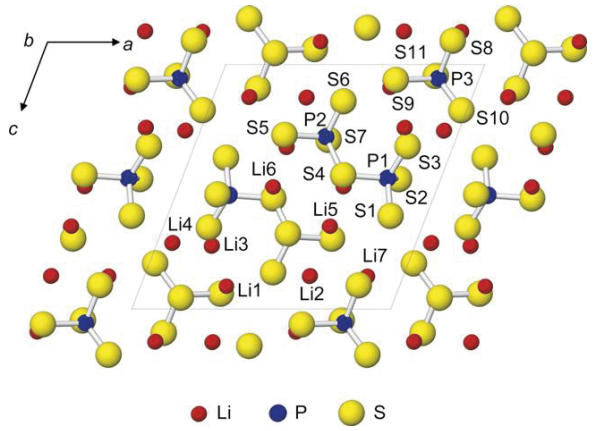

Fig. 6. Crystal structures of $Li_7P_3S_{11}$ viewed along the [010] direction. Reprinted with permission from Yamane *et al.* © 2007 Elsevier B.V.[29]

defined by its P:S ratio. Thus, the skeleton can be described by *meta*-thiodiphosphate $P_2S_6^{2-}$ moieties, which can be thought of as two edges sharing *ortho*-thiophosphate tetrahedra. The lattice parameters of the monoclinic cell are $a = 11.1156(9)$ Å, $b = 7.0070(6)$Å, $c = 6.5251(5)$Å and $\beta = 125.57(14)°$.[28]

$Li_7P_3S_{11}$ is one of the most widely studied structures among all phosphosulfide electrolytes. This material crystallizes in triclinic crystal system with space group *P*-1. It is based upon a framework consisting of tetrahedron PS_4^{3-} *ortho*-thiophosphates and corner sharing ditetrahedron $P_2S_7^{4-}$ *pyro*-thiodiphosphate groups, which play a role of finite clusters. Li cations located between the polyhedral cavities and coordinated to 3–4 sulfur atoms (Fig. 6).[29,30] PS_4^{3-} *ortho*-thiophosphate and $P_2S_7^{4-}$ *pyro*-thiodiphosphate are present in 1:1 ratio. The lattice constants of the triclinic cell as determined by synchrotron X-ray diffraction are $a = 12.5009(3)$Å, $b = 6.03160(17)$Å, $c = 12.5303(3)$Å, $\alpha = 102.845(3)°$, $\beta = 113.2024(18)°$, $\gamma = 74.467(3)°$.[29]

Upon heating, Li_3PS_4 undergoes a phase transition $\gamma \rightarrow \beta \rightarrow \alpha$ at transition temperatures of 300°C and 473°C.[31] The low temperature γ-phase has the space group $Pnm2_1$ and is isostructural to Li_3PO_4.[31] The β-phase crystallizes in *Pnma* space group, and the high temperature α-phase was first attributed to space group *Pbcn*.[32] All of them are orthorhombic. Recent detailed analysis of the structure of the α-phase indicates that the structure is actually orthorhombic *Cmcm*, which is a subgroup of *Pnma*, the space group of the β-Li_3PS_4.[33] When referring to the orthorhombic structures, it should be noted that the lattice volume increases with

Table 1. Li_3PS_4 lattice parameters of α, β and γ phase with cell volumes and cell volumes normalized to Z = 2.

Li_3PS_4	Space group	*a* (Å)	*b* (Å)	*c* (Å)	Cell volume CV (Å^3)	Normalized CV (Å^3)
α-phase @ 906 K	*Pbcn*	8.6125	9.0211	8.4262	654.66707	654.66707
β-phase @ 637 K	*Pnma*	12.8190	8.2195	6.1236	645.2178	645.21783
γ-phase @ 297K	$Pnm2_1$	7.70829	6.53521	6.1365	309.12799	618.25598

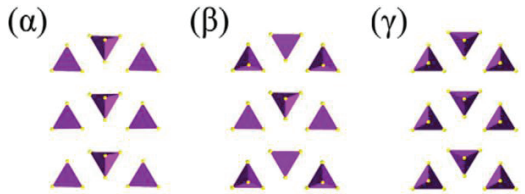

Fig. 7. Orientation of the PS_4^{3-} tetrahedra in the crystal structures of α, β and γ-phase of Li_3PS_4. Reprinted with permission from Homma *et al.* © 2010 Elsevier B.V.[31]

temperature from the γ to the α-phase; the lattice parameters and volumes are summarized in Table 1. On cooling, the transformation shows hysteresis whereby the β-phase tends to transform to γ-phase below 195°C. It is an open discussion if in microcrystalline Li_3PS_4, the β-phase can be stabilized down to ambient temperature without changes in the chemical composition. The crystal structures of α, β and γ-phase Li_3PS_4 are shown in Fig. 7.

Corresponding to the P:S ratio of 1:4, all of them have exclusively isolated *ortho*-thiophosphate PS_4^{3-} tetrahedra as structural building blocks. The polymorphs however differ with respect to the orientation of the PS_4^{3-} tetrahedra. The γ-phase has an ordered orientation with the apex pointing in the same direction (T^+ or T^- only, where T^+ and T^- indicate if the apex of the tetrahedron is up or down, respectively) as seen in Fig. 8(b). In contrast, in the β-phase, the T^+ and T^- are arranged in a zig-zag arrangement as seen in Fig. 8(a). This means that for the γ-phase, the Li^+ ions are only situated in the tetrahedral sites while in the β-phase, due to the zig-zag arrangement, the lithium ions are situated in both the octahedral and tetrahedral sites.[31]

Two polymorphs, a low temperature (LT) modification stable at $T < 210$°C and a high temperature (HT) modification were reported for Li_7PS_6.[34] The LT polymorph is orthorhombic with space group $Pna2_1$, the HT polymorph is cubic with space group F-43m. The latter is an Argyrodite structure with lattice constant $a = 9.993$Å.[34] As the P:S ratio for the Li_7PS_6 material is 1:6, the high sulfur content cannot be completely accommodated in PS_4^{3-} tetrahedra; in addition to the *ortho*-thiophosphate building blocks, there are S^{2-} anions in the lattice.[20]

Different structures have been proposed for $Li_4P_2S_6$. As phosphorus is present in formal charge state P^{4+} in this material, the structural building blocks do not consist of P_xS_y tetrahedral units, but $P_2S_6^{4-}$ anions. Early reports described the overall structure of $Li_4P_2S_6$ in terms of the space group $P6_3/mcm$ (#193).[23] Comparative analysis of this structure *vs.* its subgroup P-31m and *Pnma* by combining synchrotron X-ray diffraction and spectroscopy indicated that $Li_4P_2S_6$ possesses a space group P-31m (Fig. 8(c)). The lattice constants determined for the P-31m space group are $a = b = 6.0773(5)$Å and $c = 6.5985(6)$Å.[24]

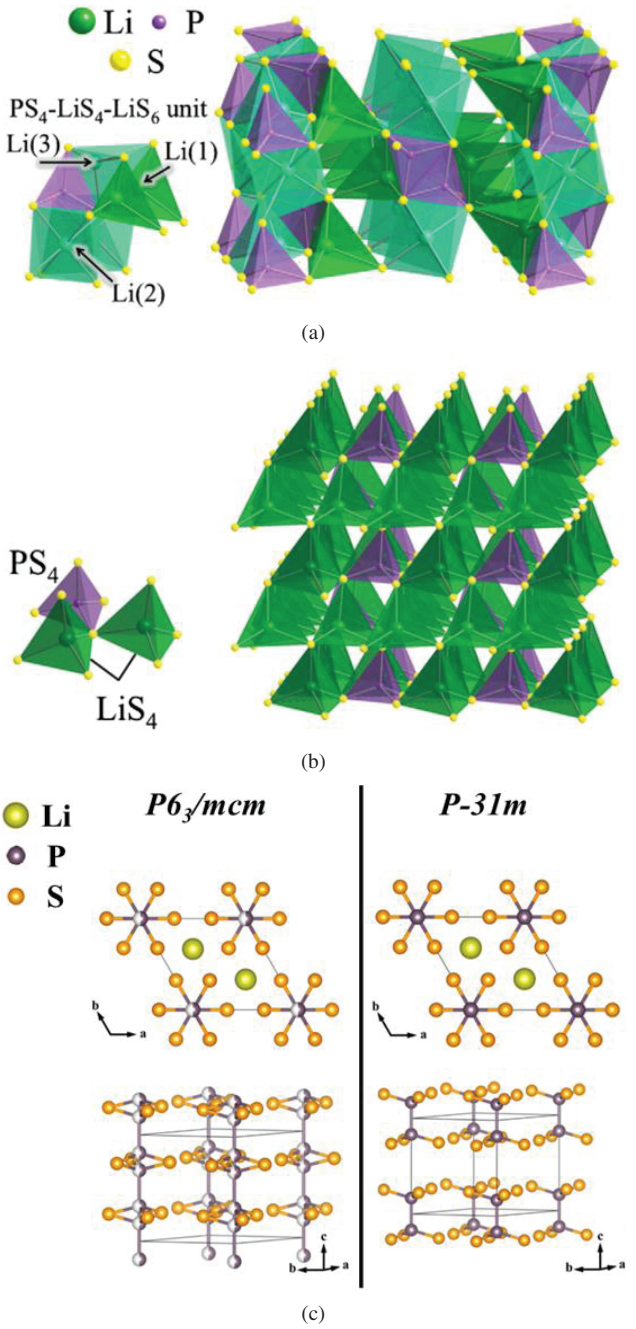

Fig. 8. Arrangement of (a) β phase and (b) γ phase. (c) Possible structures of $Li_4P_2S_6$ with $P63/mcm$ initially reported and P–31m reported by Dietrich *et al.* (a) and (b) Reprinted with permission from Homma *et al.* © 2010 Elsevier B.V.[31] (c) Adapted with permission from Dietrich *et al.* © 2016 American Chemical Society.[24]

3.3. *Li–P–S processing*

A wide scope of synthesis methods for Li_2S–P_2S_5 type electrolyte materials encompassing approaches, (i) by solid-state routes with either crystalline or previously amorphized educts, (ii) by preparation methods from melts and (iii) by liquid phase synthesis with a broad span with respect to the solvents applied, have been forwarded. Typically, processes need to be carried out in inert conditions, most commonly in

an argon filled glove box, as the starting materials are hygroscopic and sensitive to air.[35] Recent results indicate that for certain materials, processing in a dry room may be viable.[36–40] Another point of note is the careful selection of solvents and binders in order to ensure chemical stability of the phosphosulfide electrolyte.[14,15,41–43]

In a straightforward solid-state route, stoichiometric ratios of Li_2S and P_2S_5 are mixed and then crystallized at temperatures between 550°C and 700°C.[22,31,34] As high processing temperatures may render it difficult to prevent sulfur evaporation and maintain the stoichiometry, an approach according to which the educts are first amorphized by mechanical milling and subsequently re-crystallized is applied. The method originates from the procedures used in the synthesis of glasses and glass ceramics. In contrast to these processes, in which no or only partial crystallization is required, the objective of the subsequent heat treatment is a complete crystallization of the materials. According to these methods, intense milling of the educts results in the desired material after passing through the intermediate stages with $P_2S_6^{4-}$, $P_2S_7^{4-}$ and PS_4^{3-} as building blocks.[12] Ideally, the resultant material is a completely amorphized "glassy" material, for which the crystallization is accomplished at significantly lower temperatures (200–300°C) compared to processes using crystalline educts.

Historically the first synthesis of materials from the Li_2S–P_2S_5 system were conducted by Mercier *et al.* in 1982 by melting educts Li_2S and P_2S_5 for homogenization at high temperatures (950°C/1 h) in a first step.[23,44] Crystalline Li_3PS_4 was created by subsequent slow cooling, including an extended dwell time of 48 h at 500°C.[23] A slight variant of this route was applied for the synthesis of $Li_4P_2S_6$. The melt was quenched to 25°C in order to freeze the amorphous state before recrystallizing the material at 500°C.[23]

Synthesis by liquid phase reactions follows two different routes with respect to the form in which the product is yielded, distinguishing liquid phase synthesis and solution processes. In the former, the precursors added to solvents result in solid (intermediate) reaction products while the solvent being supernatant. In contrast, in the latter route, the products are present in dissolved form in the solvent.[14]

Criteria for the design of the processes that have to be taken into account are (i) the solubility of the reactants, the intermediates and the products, (ii) their stability in the solvents, (iii) the complexation of the products with the solvent and the subsequent removal of the solvent component and (iv) the crystallization behavior.[10] There are recent excellent reviews on these topics.[10,14] One critical requirement for the solvent is to avoid the formation of any hydrogen–sulfur species. There is a wide variety of organic solvents such as acetonitrile (ACN), ethyl acetate (EA), ethyl propionate (EP), dimethyl carbonate (DMC) 1,2dimethoxyethane (DME), tetrahydrofuran (THF) and anhydrous ethanol to name a few. After mixing and reacting, the solvent is removed and the compound is formed by heating, generally at low temperature (60–250°). The lower limit for the heat treatment temperature in these processes is in many cases defined by the conditions required for complete evaporation of the solvent, which may co-crystallize with the product rather than the crystallization of the materials. An advantage of the liquid phase synthesis is that it may result in homogeneous and nanostructured powders. In addition to that the products of the solution processes before heat treatment along with favorable wetting properties can be used for coating or infiltration processes in electrode fabrication.

While from a very general point of view, the solid state and the liquid processing methods applied for the synthesis of $Li_2P_2S_6$, $Li_4P_2S_6$, $Li_7P_3S_{11}$, Li_3PS_4, and Li_7PS_6 are similar, there are some specific issues for each composition.

Solid-state preparation of $Li_7P_3S_{11}$ requires relatively intensive ball milling (40 h at 500 rpm). The milled powder is enclosed in a stainless steel tube, which is sealed under Ar atmosphere. Heat treatment at 300°C for 2 h, followed by cooling to ambient temperature results in a mostly glass ceramic material. An efficient method for liquid phase synthesis of $Li_7P_3S_{11}$ from Li_2S and P_2S_5 powders is by mixing appropriate amounts in DME solvent, producing a precursor, which is a mixture of solvated Li_3PS_4 and $Li_4P_2S_7$. After vacuum drying of the precursor, crystalline $Li_7P_3S_{11}$ is obtained by heat treatment at 280°C for 1 h in Ar.[30]

Synthesis of Li_3PS_4 following a conventional solid-state route results in the γ-phase of Li_3PS_4. However, by hot pressing the glassy precursor, the phase of the Li_3PS_4 product depends on the temperature applied. When temperatures of 300°C are applied, γ-phase crystals are precipitated, however when 170–250°C are applied, β-phase is precipitated instead, and this β-phase is maintained at ambient temperature.[45] Several successful approaches to prepare β-Li_3PS_4 are provided by liquid phase synthesis. Li_3PS_4 synthesized via a THF liquid phase reaction followed by a heat treatment at 140°C is creating β-Li_3PS_4, which is stable over a wide range of temperatures.[46] The synthesized Li_3PS_4 is nanoporous in nature on the transitioning from an amorphous to a β-Li_3PS_4 crystalline structure. Using ACN solution, Li_3PS_4 results in the formation of β-Li_3PS_4 nanoflakes.[47] Li_3PS_4 from a liquid phase process using EA as the synthetic medium brings about Li_3PS_4–2EA powder, which is transformed on heat treatment at 170°C to β-Li_3PS_4.[48] A naphthalene-aided THF process provides the possibility to integrate Li_2S synthesis concomitant to the β-Li_3PS_4.[49]

As for most other Li_2S–P_2S_5 type materials, these components are the educts for solid-state synthesis of Li_7PS_6. However, higher temperatures (550°C) and extended dwell times up to 120 h are specific for this material.[34] Alternatively,

Li_7PS_6 can be obtained by reacting $Li_8P_2S_9$ with Li_2S. $Li_8P_2S_9$ can be synthesized by heating stoichiometric ratios of Li_2S, red phosphorus and sulfur in a vacuum sealed ampule at 600°C.[50] The resultant $Li_8P_2S_9$ is then reacted with Li_2S at 600°C to form Li_7PS_6 according to the reactions $4Li_2S + 2P + 5S \rightarrow Li_8P_2S_9$ and $Li_8P_2S_9 + 3Li_2S \rightarrow 2Li_7PS_6$.

Recently, a two-step liquid synthesis route for Li_7PS_6 has been developed.[51] In the first step, β-Li_3PS_4 is synthesized by dissolving stoichiometric amounts of Li_2S and P_2S_5 in ACN. The mixture is then filtered and dried at 80°C under vacuum, then heat treated to 200°C. In the second step, stoichiometric amounts of Li_2S and β-Li_3PS_4 are then dissolved in anhydrous ethanol. The mixture was then dried at 90°C under vacuum, then heat treated to 200°C, which resulted in agglomerates of nanosized granular *F*-43*m* structured Li_7PS_6 primary particles.

Crystalline $Li_2P_2S_6$ was synthesized via solid-state synthesis.[28] The importance of temperature control during the milling step, complete amorphization of the Li_2S–P_2S_5 and heat treatment applied to a pressed pellet 270°C for 20 h are emphasized to be important issues for a single phase synthesis of this material.

The composition of the $Li_4P_2S_6$ electrolyte cannot be matched with Li_2S and P_2S_5 educts. Li_2S:P_2S_5 applied in 67:33 ratio results in an $Li_4P_2S_7$ material composition. $Li_4P_2S_7$ is the intermediate product that is used in most processes for the synthesis of $Li_4P_2S_6$. Various methods have been used in the synthesis of $Li_4P_2S_6$. Excess sulfur, when reacting Li_2S and P_2S_5, can be removed via anhydrous ACN.[52] Alternatively, from $Li_4P_2S_7$ (glass) intermediate, appropriate heat treatment leading to the evaporation of part of the sulfur and reduction of phosphorus results in the formation of crystalline $Li_4P_2S_6$.[23] A third type of approach is to react Li_2S with elemental red phosphorus and sulfur.[23,24] Synthesis of $Li_4P_2S_6$ in many cases provides a mixture of crystalline and glassy phases. Depending on the processing conditions, different ratios between the crystalline and the glassy phases in $Li_4P_2S_6$ are realized. Pure glass $Li_4P_2S_6$ is formed either by high energy ball milling or melt quenching.

3.4. *Conductivity Li–P–S type*

Fair comparisons of Li-ion conductivity between different electrolytes are not straightforward even within the similar chemistries of the Li–P–S types of electrolytes. Distinguishing between the polymorphs in some of the materials has been taken into account. However, the issue that renders an analysis of the Li–P–S type materials more critical than for other materials is the tendency of the Li–P–S type materials to form secondary glass phase in addition to the crystalline material fraction. Moreover, the preparation of the samples for the conductivity measurement may have significant impact on the result. These subjects have therefore to be addressed before coming to a comparison of the materials. The discussion on Li-ion conductivity is therefore organized in three sections. In the first section, the scope of the results on Li-ion conductivity of the base materials $Li_2P_2S_6$, $Li_7P_3S_{11}$, Li_3PS_4, and Li_7PS_6 of the Li–S–P type electrolytes will be sketched and related to the challenges arising from the different phase fractions and sample preparation in these materials on the evaluation of the Li-ion conductivity. The second section addresses material-specific properties in detail. In the third section, the Li-ion conductivities are analyzed with respect to the correlations to the Li_2S–P_2S_5 ratios.

3.4.1. *Polymorphs and glassy fractions—impact on scattering of Li-ion conductivities*

The Li-ion conductivities reported for the Li_2S–P_2S_5 type base materials $Li_2P_2S_6$, $Li_7P_3S_{11}$, Li_3PS_4, and Li_7PS_6 are compiled in Fig. 9. Influenced by the different crystalline phases, glassy phase fractions and interface conditions resulting from sample preparation, the data for the conductivities for $Li_7P_3S_{11}$ and Li_3PS_4, for which several investigations on the Li-ion conductivities are available, scatter by more than one order of magnitude when related merely to the chemical compositions of the Li_2S–P_2S_5 materials.

While it is quite straightforward to distinguish between the different crystalline polymorphs of the materials, the influence of the fractional glass phase is much more difficult to identify and evaluate. In most of the synthesis methods, the stages with amorphous phase intermediate materials are involved and the glass phase remaining from intermediate stages or formed during the last high temperature steps may be present. This applies to both the solid-state processes, where the crystalline materials are formed from the melt or amorphized powders, as well as for liquid synthesis. Even if the presence of the glass phase is detectable and the phase

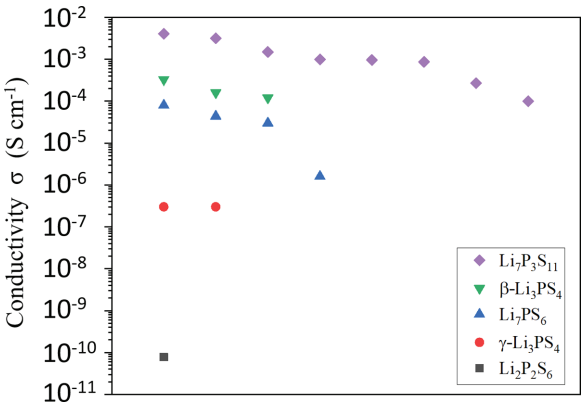

Fig. 9. Li-ion conductivities of the Li_2S–P_2S_5 type base materials $Li_2P_2S_6$, $Li_7P_3S_{11}$, Li_3PS_4, and Li_7PS_6 including glass and glass ceramic materials with the respective chemical compositions. The *x*-axis indicates the values given by various authors. Data and references can be found in Table 3.

fractions of the glass phase can be quantified, there is different impact on the conductivity depending on the form in which the glass secondary phase is present, for example, as separate glassy regions "glassy grains" or in the form of films covering the surface of the crystallites. While small fractions of glass phase confined to distinguished compact regions are expected to have only minor effects, glassy films on the surface of crystalline grains may have pronounced influence on the Li-ion conductivity. On the one hand, such a glass film will determine the interface resistance on Li-transport between different crystalline grains. On the other hand, the presence of glass as a grain boundary phase may result in a percolating network of the glass phase, which, in case of high Li-ion conductivity of this phase, provides an additional pathway for the Li-ion transport. In general, influence of glass phase components may be present in all of the materials, however, the tendency to form glass phase is different depending on the composition and processing.

In addition to the glass phase component in the materials resulting from the synthesis of the powder, the preparation of the (ceramic) samples for the conductivity measurements may have a pronounced influence on formation of the interfaces. Along with samples based on the same Li–P–S powders, cold pressing results in ceramics with substantially lower Li-ion conductivity compared to samples that are spark-plasma sintered (SPS) or hot-pressed (Fig. 10(a)).[30,45,53] Specifically, in cases of glass ceramic based material, the glass phase plays an important role in reducing the resistance between grains (Fig. 10(b)).[30]

Evaluation of the results on Li-ion conductivities for Li_3PS_4 and Li_7PS_6 has to take into account the different crystalline polymorphs. Depending on the processing conditions, Li_3PS_4 and Li_7PS_6 may crystallize either in the form of high conductive high temperature phases or adopt the low temperature modifications with substantially lower conductivities. In contrast, the wide scope of Li-ion conductivities for $Li_7P_3S_{11}$ is not due to crystalline polymorphs. In this material, the results on Li-ion conductivity will be analyzed according to the processing methods and grain/particle interface conditions related to the sample preparation. The influence of the glass phase component and the state of the interfaces are the reasons for differences in results in Li-ion conductivity amounting almost two orders of magnitude for $Li_7P_3S_{11}$. As there are only few results that are available for the conductivity of $Li_2P_2S_6$, eventual influence of processing and glass phase in this material still has to be investigated. Considering the importance of the presence of potential glass phase, the results on Li-ion conductivities of the glasses with compositions corresponding to those of the crystalline materials are integrated in the analysis.

3.4.2. *Detailed material-specific discussion of Li-ion conductivities*

$Li_7P_3S_{11}$: In the Li_2S–P_2S_5 group, the high performing crystalline $Li_7P_3S_{11}$ materials have Li-ion conductivities up to more than 10^{-3} S cm^{-1} at ambient temperature. However, there is pronounced scattering considering the scope of conductivities. When splitting up the conductivities according to the processing route the materials originate from, a clear trend is visible (Fig. 11(a)).

The Li-ion conductivities for the $Li_7P_3S_{11}$ glasses at ambient temperature are in the range between 10^{-5} and 10^{-4} S cm^{-1}. An order of magnitude higher are the conductivities for $Li_7P_3S_{11}$ synthesized by liquid phase processes, while the conductivities of most conventional glass ceramics are between 1×10^{-3} and 5×10^{-3} S cm^{-1} at ambient temperature. Hot pressing results in Li-ion conductivities that are still half

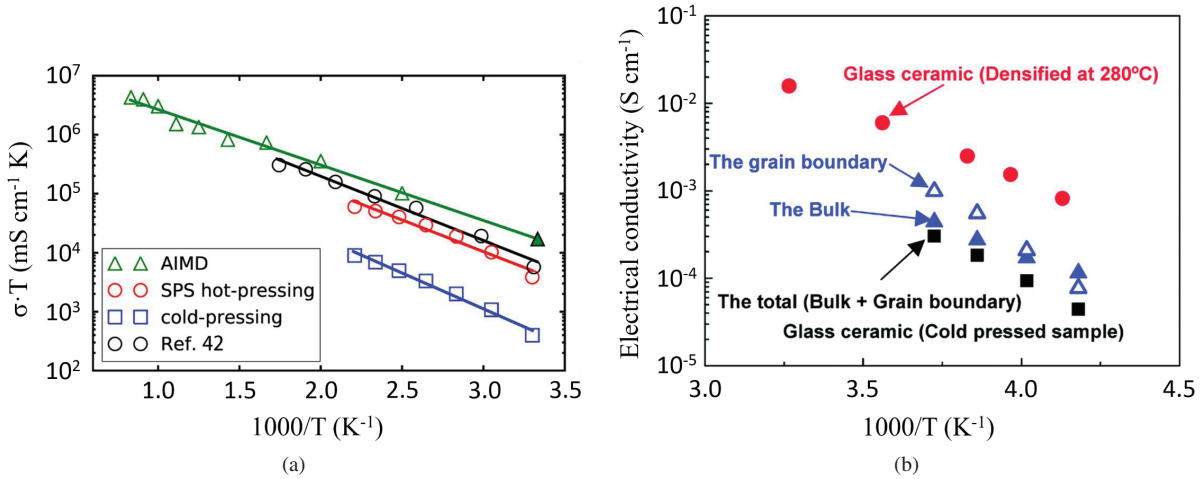

Fig. 10. (a) Conductivity of $Li_7P_3S_{11}$ depending on the preparation method (cold-pressed versus SPS hot-pressed) materials and comparison with AIMD simulations. Arrhenius plot by Seino *et al.* of $Li_7P_3S_{11}$ is shown for comparison.[54] Reprinted with permission from[53] Copyright © 2016 American Chemical Society (b) Bulk and grain boundary conductivity of the cold-pressed versus glass-ceramic material. Reproduced from[54] with permission from the Royal Society of Chemistry.

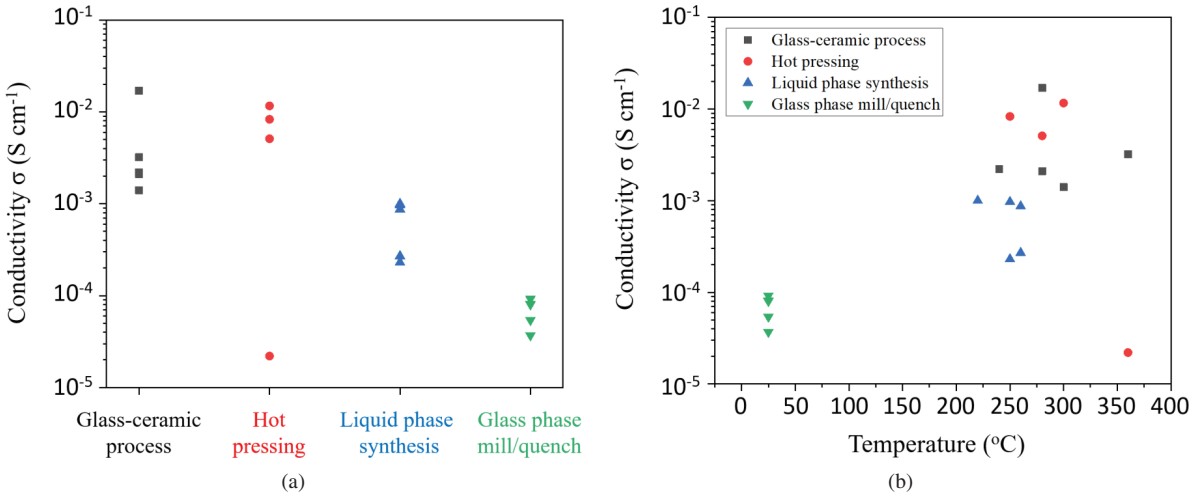

Fig. 11. Li-ion conductivities for crystalline $Li_7P_3S_{11}$ glass ceramics and $70Li_2S–30P_2S_5$ glasses: (a) according to processing methods (b) Li-ion conductivities at ambient temperature as a function of the synthesis temperatures. Data and references can be found in Table 2.

an order of magnitude higher than those of the conventional glass ceramics.

Two exceptions in Fig. 11(b) are the hot-pressed material with $\sigma = 2.2 \times 10^{-5}$ S cm^{-1} and the glass ceramic with $\sigma = 1.7 \times 10^{-2}$ S cm^{-1}. The former material demonstrates that the transition of $Li_7P_3S_{11}$ to $Li_4P_2S_6$, which is well known as "second nucleation" in the glass ceramics processes, arises also along with hot pressing at 360°C.[55] The latter one is a glass ceramic material that was subject to an optimized temperature treatment, which leads to extraordinary high performance with an ambient temperature Li-ion conductivity of 1.7×10^{-2} S cm^{-1}.[30] Concomitant to the processes, the ranges for the synthesis temperatures in the final steps are also correlated to Li-ion conductivities. While preparation at ambient temperatures, as in the case of milled glasses and liquid phase synthesized $Li_7P_3S_{11}$ processed at 230–260°C, tends to lead to lower conductivity, the processing temperatures for conventional glass ceramics and hot-pressed $Li_7P_3S_{11}$ with higher Li-ion conductivities are mostly slightly higher. The upper temperature limit for high performance material is given by the nucleation temperature for the low conducting $Li_4P_2S_6$ phase at 360°C. Depending on the process for the creation of the electrolytic powder, the sample preparation for the electrolyte pellet differs. While Li-ion conductivities of glassy materials and liquid phase processed $Li_7P_3S_{11}$ are mostly analyzed on cold compacted samples, the conductivities for glass ceramics or hot-pressed $Li_7P_3S_{11}$ are measured on denser pellets formed utilizing elevated temperatures.

Li_3PS_4: The Li-ionic conductivity of Li_3PS_4 crucially depends on the phase composition. The low temperature γ-phase has a low ambient temperature Li-ion conductivity of about 3×10^{-7} S cm^{-1}.[31,44] At elevated temperatures, in the stability range of the β-phase, the Li-ion conductivity is in the range up to 10^{-3} S cm^{-1}. When considering the values for the β-phase extrapolated to ambient temperature, the (theoretical) conductivity of the β-phase at 25°C yields 9×10^{-7} S cm^{-1}. The type of phase in which Li_3PS_4 can be realized at ambient temperature is related to the morphology and the processing.

Crystalline Li_3PS_4 transforms on cooling from the βLi_3PS_4 stability region to γ-Li_3PS_4. When Li_3PS_4 ($75Li_2S{:}25P_2S_5$) glass is hot-pressed at 300°C, γ-Li_3PS_4 is precipitated out forming a glassceramic with an ambient temperature Li-ion conductivity of 2×10^{-5} S cm^{-1}.[45] However, when a reduced temperature is used (170–250°C), β-Li_3PS_4 is precipitated out instead, which possesses a higher ambient temperature Li-ion conductivity of 1.4×10^{-4} S cm^{-1}.[45] Moreover, in nanoporous material prepared by a liquid phase THF

Table 2. Synthesis methods of $Li_7P_3S_{11}$; *T*: Synthesis temperature, MM: mechanochemical milling, HT: Heat treatment, MQ: Melt quench, HP: Hot press, LQ: Liquid synthesis route. Reported Li-ion conductivities at ambient temperature.

Process	*T* (°C)	σ (S cm^{-1})	References
MM +HT	240	2.2×10^{-3}	56
MM +HT	360	3.2×10^{-3}	56
MQ + HT	280	1.7×10^{-2}	54
MQ + HT	280	2.1×10^{-3}	57
MQ + HT	300	1.4×10^{-3}	54
HP	300	1.16×10^{-2}	53
HP	250	8.3×10^{-3}	55
HP	280	5.1×10^{-3}	55
HP	360	2.2×10^{-5}	55
LQ ACN	220	1.0×10^{-3}	58
LQ THF	250	9.7×10^{-4}	59
LQ ACN	260	8.7×10^{-4}	60
LQ DME	260	2.7×10^{-4}	30
LQ ACN	250	2.3×10^{-4}	59
MM	25	8.1×10^{-5}	55
MM	25	5.4×10^{-5}	56
MM	25	3.68×10^{-5}	61
MQ	25	9.2×10^{-5}	57
MQ	25	8.0×10^{-5}	54

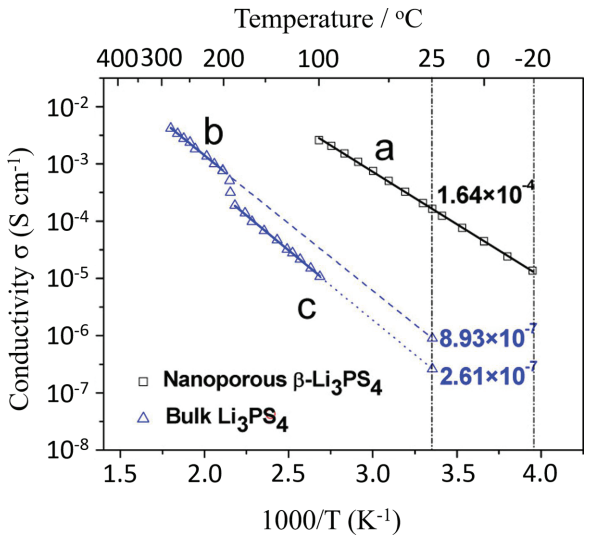

Fig. 12. Comparison of conductivities of nanoporous β-Li_3PS_4 and bulk Li_3PS_4. Reprinted with permission from Liu *et al.* Copyright © (2013) American Chemical Society.[46]

synthesis, the β-phase can be stabilized to ambient temperature, which results in an Li-ion conductivity of 1.6×10^{-4} S cm^{-1} at 25°C, that is larger by an order of three compared to Li_3PS_4 synthesized via conventional solid-state reactions (Fig. 12).[46] Recent detailed investigations of nanoporous β-Li_3PS_4 with X-ray diffraction, NMR, and Raman spectroscopy revealed the presence of additional amorphous phase and remnant solvent even after prolonged heat treatment at temperatures well above the boiling point of the solvent.[36] Analysis of the dependence of Li-ion conductivity in nanoporous β-Li_3PS_4 materials on the phase contents indicate that high conductivity is related to the content of amorphous phase.[62]

For Li_3PS_4 materials synthesized by alternative liquid phase processes, the conductivities are similarly high. For Li_3PS_4 nanoflakes formed by liquid phase synthesis using ACN solution,[47] Li_3PS_4 from a naphthalene-aided THF process with integrated Li_2S synthesis[49] and Li_3PS_4 from a liquid phase process using EA as the synthetic medium,[48] ambient temperature Li-ion conductivities are 1.2×10^{-4} S cm^{-1}, $1.0–1.8 \times 10^{-4}$ S cm^{-1} and 3.3×10^{-4} S cm^{-1}, respectively. The ambient temperature Li-ion conductivities of glass and glass ceramics with $75Li_2S{:}25P_2S_5$ composition are 1.7×10^{-4} S cm^{-1} and 2.8×10^{-7} S cm^{-1}, respectively.[63]

$Li_2P_2S_6$: The Li-ion conductivity of the $Li_2P_2S_6$ material at ambient temperature is as low as 7.8×10^{-11} S cm^{-1} with a high activation barrier of 0.48 eV. The low Li-ion conductivity has been explained by the crystal structure as the structure only allows for one-diamensional conducting chains.[28] The inherently low Li-ion conductivity and high activation energy of $Li_2P_2S_6$ renders it not very suitable as a solid-state electrolyte in an all-solid-state battery. Also, the Li-ion conductivity of glasses with 50:50 $Li_2S{:}P_2S_5$ ratio is lower than for glasses with higher Li_2S fraction.[44]

Li_7PS_6: High- and low-temperature modifications of the structure are also present in Li_7PS_6. Ambient temperature measurements for Li_7PS_6 in its low temperature $Pna2_1$ phase indicate an ambient temperature Li-ion conductivity of 1.6×10^{-6} S cm^{-1}.[64] These results were obtained on cooling after a first heating run to 277°C during which the material temporarily transformed to the high temperature cubic *F*-43*m* phase. The ambient temperature conductivity of the Li_7PS_6 in the low temperature state after the heating cycle was substantially higher than the conductivity of the Li_7PS_6 (<10^{-7} S cm^{-1}) in an "as prepared by coldpressing state" at the beginning of the thermal cycle. The increase in conductivity along with the heating cycle could in part be due to enhanced densification of the sample concomitant to the elevated temperatures. At temperatures higher than 210°C, the structure transforms to the high temperature cubic phase. In the high temperature *F*-43*m* phase, the ambient temperature Li-ion conductivity is 3×10^{-5} S cm^{-1} at 300°C.[64] In glassy powders corresponding to $87.5Li_2S–12.5P_2S_5$, which are produced by mechanically milling for 40 h, the Li-ion conductivity is 4.4×10^{-5} S cm^{-1} at ambient temperature.[21]

$Li_4P_2S_6$: $Li_4P_2S_6$ has been reported to have an ambient temperature Li-ion conductivity in the range of 10^{-10} to 10^{-6} S cm^{-1}. The wide range of conductivity for $Li_4P_2S_6$ is due to the fact that it exists as a mixture of crystalline and glassy phases, in which the crystalline portion of $Li_4P_2S_6$ has poor Li-ion conductivity, while the glassy areas have high Li-ion conductivity.[24] The different fractions of crystalline and glassy phases in $Li_4P_2S_6$ produced by various processing methods lead to the wide range of reported Li-ion conductivities. As crystalline $Li_4P_2S_6$ has quite low Li-ion conductivity, the $Li_4P_2S_6$ samples that have a higher glass content exhibit a higher Li-ion conductivity, implying that a purely glass $Li_4P_2S_6$ sample formed either by high energy ball milling or melt quenching would have much higher Li-ion conductivities when compared to their polycrystalline counterparts.

$Li_{3+5x}P_{1-x}S_4$ series: The materials of the $Li_{3+5x}P_{1-x}S_4$ series cover $Li_2S{:}P_2S_5$ ratios 75:25 to 87.5:12.5 for $0 \le x \le 0.33$ between Li_3PS_4 and Li_7PS_6. In this range, the Li-ion conductivities are subject to pronounced changes with composition (Fig. 13). A moderate increase in Li-content in Li_3PS_4 leads to a substantial increase in conductivity (region I) that peaks in a narrow region at $Li_{3+5x}P_{1-x}S_4$ ($0.04 \le x \le 0.07$ approximately) where it amounts up to 1.5×10^{-4} S cm^{-1} for $Li_{3.325}P_{0.935}S_4$ (region II). Along with a further increase in x (or the $Li_2S{:}P_2S_5$ ratio), the Li-ion conductivities first decrease sharply toward $Li_4P_{0.8}S_4$ ($Li_{10}P_2S_{10}$) (region III) before they recover again with compositions approaching Li_7PS_6 (region IV), but without reaching the high levels of the region II materials. The change of the conductivities among the $Li_{3+5x}P_{1-x}S_4$ materials goes along with structural changes that are not completely

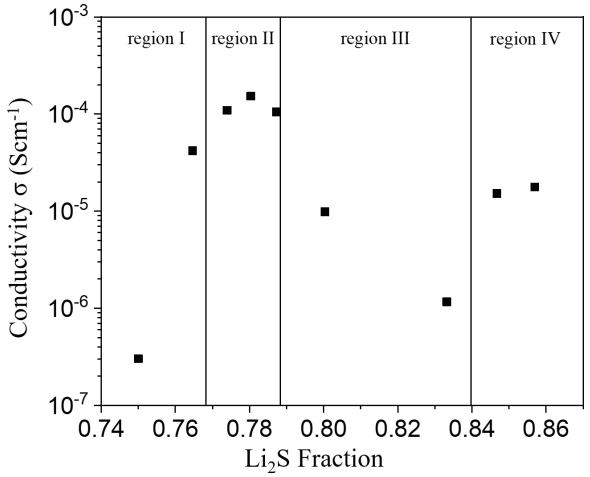

Fig. 13. Ambient temperature Li-ion conductivity of the materials from the Li-interstitial doped $Li_{3+5x}P_{1-x}S_4$ series. Plotted from data from Murayama *et al.*[22]

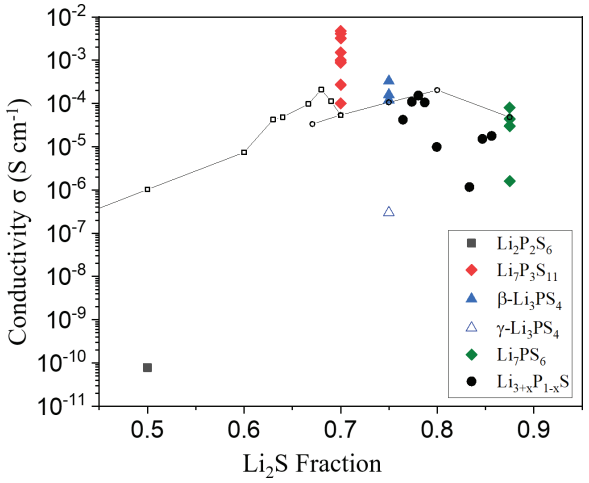

Fig. 14. Li-ionic conductivity at ambient temperatures of Li_2S–P_2S_5 type materials depending on the Li_2S–P_2S_5 fraction. Data and references can be found in Table 3. The benchmark lines for glasses are based on results by Tatsumisago *et al.*[21,65] (empty circle) and Tachez *et al.* (empty square).[44]

understood so far. The structural changes are correlated to the conductivities, as it seems clear that in the region II, a structure different from those of the Li_3PS_4 is realized.[22]

Superionic crystals with structures similar or even equal to those of the $Li_{3+5x}P_{1-x}S_4$ region II electrolytes can be synthesized also via a glass ceramic process. The ambient temperature Li-ion conductivity of electrolyte material prepared from mechanically milled $80Li_2S{:}20P_2S_5$ glass along with 240°C heat treatment is 7.2×10^{-4} S cm^{-1} on cooling after a conductivity measurement run to 230°C.[63]

$Li_{9.6}P_3S_{12}$: The very high Li-ion conductivities of the electrolyte $Li_{3.25}P_{0.95}S_4$ from the $Li_{3+5x}P_{1-x}S_4$ series are still overrun by the performance of $Li_{9.6}P_3S_{12}$.[27] The ambient temperature Li-ion conductivity of this material, in which in contrast to the $Li_{3+5x}P_{1-x}S_4$ series, the additional Li-content is not compensated by a reduction in phosphorus content, is 1.2×10^{-3} S cm^{-1}.[27] Its structure has been attributed to the LGPS type, this however is still under discussion.

3.4.3. *Li-ion conductivities related to Li_2S–P_2S_5 fraction*

An overview of the Li-ion conductivities of Li_2S–P_2S_5 type materials as a function of the ratio of this component is provided in Fig. 14. The data (Table 3) include conductivities of crystalline electrolytes, glass ceramics and glasses in the form of specific compositions. In addition, the conductivities of most characteristic glasses with the respective compositions are indicated in the form of lines in the diagram.[44,65]

The diagram indicates that the highest conductivities for crystalline and glass ceramic electrolytes are realized with $Li_7P_3S_{11}$ materials at $70Li_2S{:}30P_2S_5$. In the region with $Li_2S{:}P_2S_5$ less than 70:30 for crystalline materials and for glasses below 65:35, the Li-ion conductivities are relatively low. The Li-ion conductivities for the electrolytes with high $Li_2S{:}P_2S_5$ ratios, i.e., 75:25 for Li_3PS_4, 75:25 to 87.5 for the $Li_{3+5x}P_{1-x}S_4$ series and 87.5:12.5 for Li_7PS_6 are quite difficult to evaluate. While the data indicate an Li-ion conductivity for Li_3PS_4 higher than for the two latter types of materials, it has to be taken into account that the high conductivities for the Li_3PS_4 have been realized with hot-pressed or nanostructured materials that could be stabilized in the high temperature phase, which is considered to be more

Table 3. Li-ion conductivity and activation energies of $Li_xP_yS_z$ type materials at ambient temperature unless otherwise stated.

Stoichiometry	σ (S cm^{-1})	E_a (eV)	References
Li_3PS_4 β-phase	3.3×10^{-4}	0.37	48
Li_3PS_4 β-phase	1.6×10^{-4}	0.36	46
Li_3PS_4 β-phase	1.2×10^{-4}	0.36	47
Li_3PS_4 β-phase	3.0×10^{-2} (227°C)	0.16	31
Li_3PS_4 β-phase (glassceramic)	1.4×10^{-4}	—	45
Li_3PS_4 γ-phase	3.0×10^{-7}	0.49	31
Li_3PS_4 γ-phase	3.0×10^{-7}	0.49	44
Li_3PS_4 γ-phase (glassceramic)	1.4×10^{-4}	—	45
$Li_2P_2S_6$	7.8×10^{-11}	0.48	28
$Li_4P_2S_6$	2.38×10^{-7}	0.29	52
$Li_4P_2S_6$	1.6×10^{-10}	0.48	24
$Li_7P_3S_{11}$	4.1×10^{-3}	0.15	66
$Li_7P_3S_{11}$	3.2×10^{-3}	0.12	29
$Li_7P_3S_{11}$	1.5×10^{-3}	0.24	67
$Li_7P_3S_{11}$	1.0×10^{-3} (22°C)	0.13	58
$Li_7P_3S_{11}$	9.7×10^{-4}	0.32	59
$Li_7P_3S_{11}$	8.7×10^{-4}	0.37	60
$Li_7P_3S_{11}$	2.7×10^{-4}	0.39	30
$Li_7P_3S_{11}$	1.0×10^{-4}	—	68
$Li_{9.6}P_3S_{12}$	1.2×10^{-3}	—	27
Li_7PS_6 ht	3.0×10^{-5} (300°C)	0.35	64
Li_7PS_6 glass	4.4×10^{-5}	0.42	21
Li_7PS_6 crystal	8.0×10^{-5}	—	21
Li_7PS_6 lt	1.6×10^{-6} (40°C)	0.16	64

favorable for the Li-conduction. Both the characteristics are not available for the Li_7PS_6 material. The results on the Li-ion conductivity for the Li_7PS_6 is related to the low temperature phase, while conductivity measurements at 550°C indicate an enhanced conductivity for the high temperature *F*-43*m* phase. The materials investigated in the $Li_{3+5x}P_{1-x}S_4$ series were prepared by solid-state route or conventional glass ceramic processes. Thus, the evaluation of the electrolytes with the most favorable performance in the region Li_2S:P_2S_5 remains an open question.

4. Thio-LiSICon Electrolyte Materials

The development of the phosphosulfide electrolytes originated from two sources, the knowledge on Li_3PS_4 electrolyte with its β- and γ-polymorphs being archetypes for the thio-LiSICons and the preceding development of oxide LiSICon such as Li_3PO_4, Li_4SiO_4, Li_4GeO_4 and $Li_{14}Zn(GeO_4)_4$. The thio-LiSICon group of electrolytes with its prototype materials $Li_{4-x}M'_{1-y}M''_yS_4$ comprises a much wider scope of compositions than merely "true phosphosulfide" electrolytes. With both M′ and M″ other than phosphorus, but with M′, M″= Ge, Al, Zn, Ga and Sb, it encompasses materials that can be described as sulfur-based electrolytes containing lithium and one (M′=M″) or two (M′≠M″) semi-metallic or metallic elements. Moreover, materials with stoichiometry different from prototype $Li_{4-x}M'_{1-y}M''_yS_4$, but isostructural with or structures close to *Pnma* and *Pnm*21, such as $Li_{4-2x}Zn_xGeS_4$, are also labeled thio-LiSICon.

Following the concept of designing electrolyte materials based on high-polarizing sulfur-based polyanions suggested by Kanno *et al.*,[17] substituting the oxygen by sulfur resulted first in electrolyte materials such as Li_4GeS_4 and a revival of the previously known Li_4SiS_4 as sulfide counterparts of Li_4GeO_4 and Li_4SiO_4 (Fig. 15).[3] Based on the idea to enhance the amount of mobile Li-ions, follow-up development of the base materials Li_4GeS_4 and Li_4SiS_4 by aliovalent doping was forwarded with the objective to induce either vacancies or interstitials in order to enhance the Li-ion transport. Thereby, three types of doping strategies for the Li_4MS_4 electrolytes were pursued (Fig. 15): (i) partial replacement of the M^{4+} cation in the Li_4MS_4 electrolytes by phosphorus, considered as P^{5+} within this concept, along with concomitant reduction in the Li^+ content (ii) partial replacement of Li^+ by an M^{2+} ion such as Zn^{2+} along with charge compensating reduction of the lithium. Common objective of both these approaches was to create Li-vacancies in the materials. (iii) partial replacement of the M^{4+} cation in the Li_4MS_4 by an M^{3+} cation, such as Al^{3+} or Ga^{3+}, whereby the charge compensation was accomplished by a corresponding increase in lithium content. The intention for this approach was to create lithium interstitials.

The first "true phosphosulfide" electrolytes of the thio-LiSICon type were $Li_{4-x}Ge_{1-x}P_xS_4$ compounds, reported by Kanno and Murayama in 2001.[4] Recently, new approaches to further improve the thio-LiSICon electrolytes in the sulfur-based LiSICon system have been addressed. Tin-based electrolytes were synthesized and examined with results published under the label lithium-chalcogenidotetrelates with Li_4SnS_4 termed "tetralithium *ortho*-sulfidostannate."[69] Partial isovalent substitution of germanium in Li_4GeS_4 by Sn according to the stoichiometry $Li_4Ge_{1-x}Sn_xS_4$ was addressed for tin contents $0 \le x \le 0.75$. Both the approaches resulted in innovative thio-LiSICon structured *Pnma* materials with good conductivities, but without outperforming the Li-ion conductivity of $Li_{4-x}Ge_{1-x}P_xS_4$.

4.1. *Chemistry and phase relations of thio-LiSICon materials*

In both the systems, Li–S–Si (Fig. 16(a)) and Li–S–Ge (Fig. 16(b)), two ternary and several binary compounds are

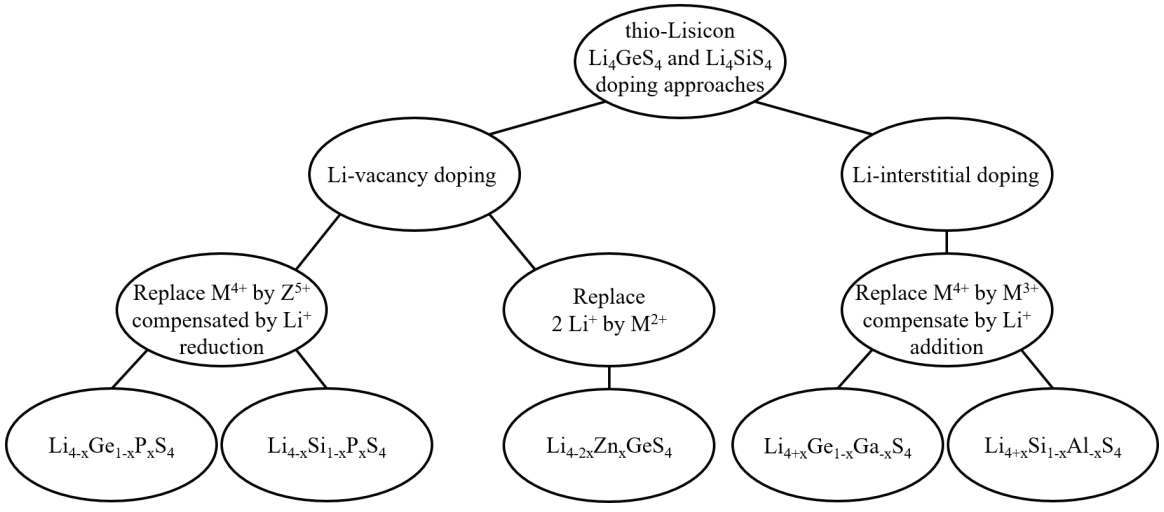

Fig. 15. Aliovalent doping strategies for thio-LiSICon electrolytes Li_4GeS_4 and Li_4SiS_4.

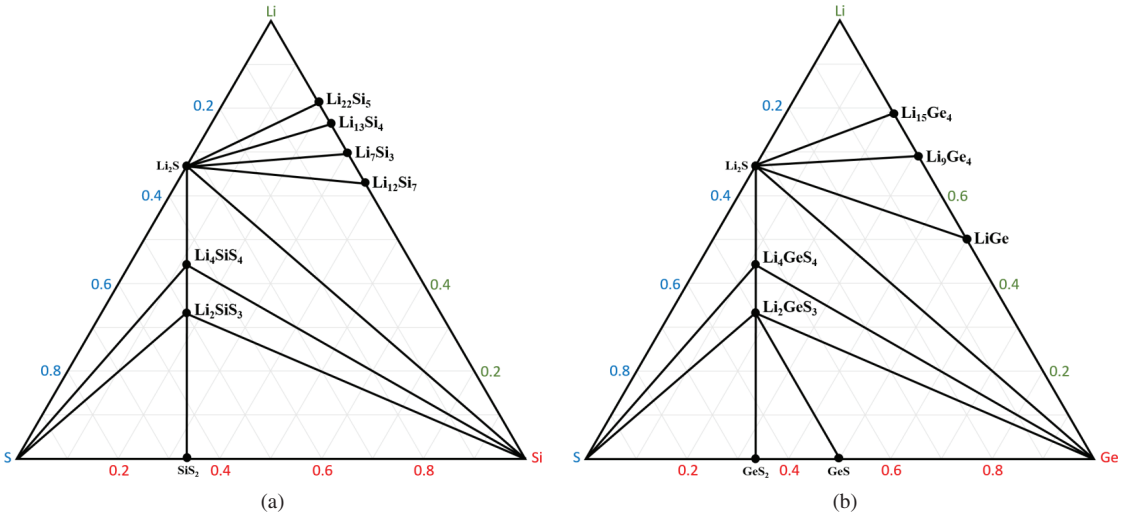

(a) (b)

Fig. 16. (a) Ternary phase diagram Li–S–Si and (b) Ternary phase diagram Li–S–Ge, Scales are in mol.%.

known. The most important materials for the thio-LiSICon are Li_2S and SiS_2, which, in a 2:1 ratio, are the constituents of the Li_4SiS_4 electrolytes. Another Li-conducting electrolyte Li_2SiS_3 is on the Li_2S–SiS_2 tie line as well (Li_2S:SiS_2 = 1:1). There are four stable binary lithium–silicon materials with Li:Si ratios ranging from 22:5 to 7:3 (4.4 to 2.33).[3] The region of interest for the lithium-ion conducting materials, the tie line between the semi-metal disulfide and Li_2S is very similar in the Li–S–Ge and the Li–S–Si system. The Li_2S–GeS_2 tie line contains two Li-ion conductors Li_4GeS_4 and Li_2GeS_3. Li–Ge binary compounds however exist with stoichiometries different from those of the binary Li–Si materials. In addition to the germanium disulfide, there is also a monosulfide GeS for this semi-metal.

The characteristics of the dopant approaches for the Li_4MS_4 (M = Si, Ge, Sn) can be discussed using the ternary phase diagrams. First, the changes in lithium stoichiometry along with doping can be displayed in a phase diagram with components Li_2S, and semi/metal sulfide components, whereby the components are given in a form containing two moles of semi/metals. All compositions $Li_4MM'S_4$ (M^{4+}, M'^{4+}), $Li_{4+x}M''_x\,M_{1-x}S_4$ (M^{4+}, M''^{3+}) and $Li_{4-x}M_{1-x}P_xS_4$ (M^{4+}, P^{5+}) lie on the tie lines indicated exemplarily by Li_4GeS_4–Li_4SnS_4, Li_4GeS_4–Li_5AlS_4 and Li_4GeS_4–Li_3PS_4, respectively (Fig. 17(a)). For isovalent substitution of tetravalent elements Si, Ge and Sn, the lithium content remains the same. When doping the LiSICOns based on tetravalent semi/metals with trivalent cations, the lithium content has to be increased, and along with doping via pentavalent phosphorus, the lithium content has to be reduced in order to compensate the charges.

Considering the elemental phase diagrams Li–S–M, it is visualized that from a stoichiometric point of view, the arrangement of the anionic substructure in isolated $M'S_4$

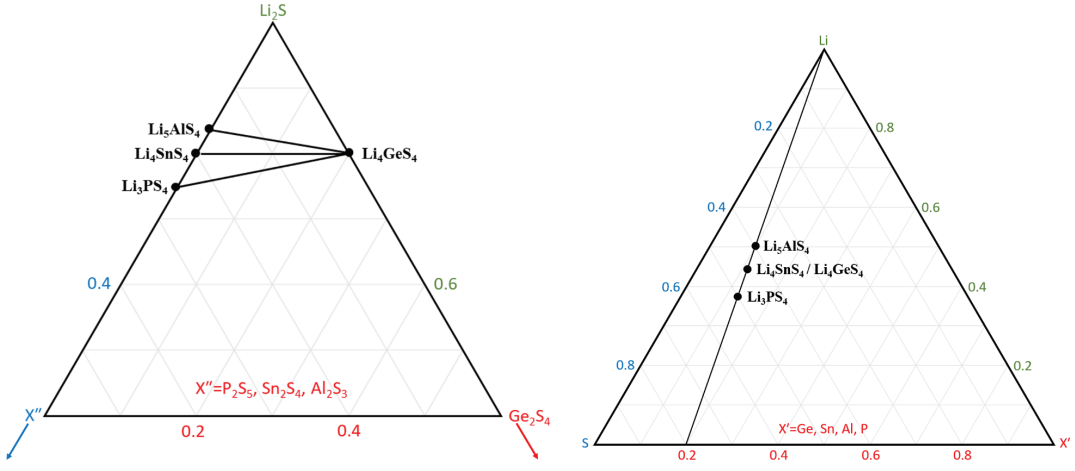

(a) (b)

Fig. 17 (a) Ternary phase diagram Li_2S–X″–Ge_2S_4 with X″ normalized to sulfides containing two semi/metal atoms (b) ternary phase diagram Li–S–X′ with X′ = Ge, Sn, Al, P. Scales are in mol.%.

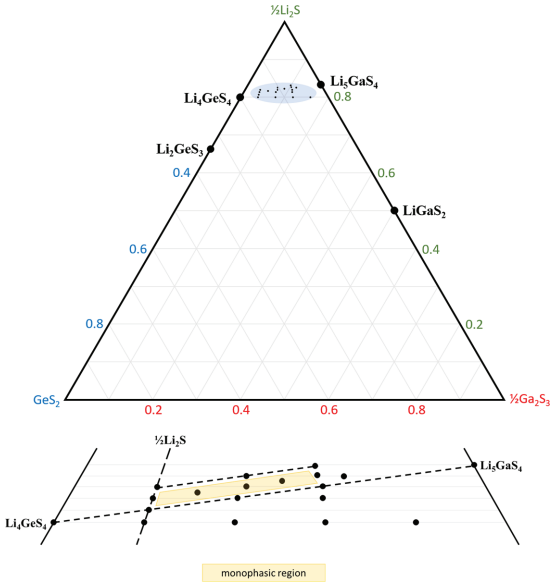

Fig. 18. Ternary phase diagram Li_2S–GeS_2–½Ga_2S_3 indicating the single phase materials $Li_{4+x+\delta}Ge_{1-x-\delta}Ga_xS_4$. Scales are in mol.%. Data from Kanno *et al.*[17]

tetahedra can be realized (Fig. 17(b)). All the components used in the binary doping systems lie on the tie line Li–PS_4. Thus, the S/(M+M′+P) ratio of 4:1 is maintained, whatever the ratio between components Li_4MS_4, $Li_5M'S_4$ and Li_3PS_4 realized. The Li:S ratio of Li_4MS_4 with 1:1 is in between those of Li_3PS_4 and Argyrodite-type Li_7PS_6 (1.16:1). For the electrolytes in the Li_4MS_4–$Li_5M'S_4$ systems, the Li:S ratios amount up to 1.25:1 for the $Li_5M'S_4$. The 1.16:1 Li:S ratio as for the Argyrodite-type Li_7PS_6 is realized in $Li_{4+x}M''_xM_{1-x}S_4$ (M^{4+}, M''^{3+}) at $x = 0.64$.

While many of the doped Li_4SiS_4, Li_4GeS_4 and Li_4SnS_4 electrolytes compositions, corresponding to those indicated by the tie lines Li_4MS_4–$Li_5M'S_4$ (M = Al, Sb) and Li_4MS_4–Li_3PS_4, result in phase pure materials, the case of doping with Gallium stoichiometry has to be slightly modified. Figure 18 indicates the range of nominal compositions, which result in single phase $Li_{4+x+\delta}Ge_{1-x-\delta}Ga_xS_4$ electrolytes along with preparation by a solid-state route from Li_2S, GeS_2 and Ga_2S_3 for which slightly higher lithium content is required.[17] Similarly, for Al doping of Li_4GeS_4 and Li_4SnS_4 to form the intended electrolyte compositions of $Li_{4.4}Al_{0.4}Ge_{0.6}S_4$ and $Li_{4.4}Al_{0.4}Sn_{0.6}S_4$, the Li_2S content in the synthesis has to be reduced by 5 mol.% in order to avoid the formation of an Li_2S impurity phase. The nominal stoichiometry of these electrolytes thus corresponds to $Li_{4.18}Al_{0.4}Ge_{0.6}S_{3.89}$ and $Li_{4.18}Al_{0.4}Sn_{0.6}S_{3.89}$, respectively.[70]

4.2. *LiSICon structure*

In the base materials Li_4SiS_4, Li_4GeS_4 and Li_4SnS_4, building blocks of the anionic structure consist of tetrahedrally arranged sulfur atoms centered by the tetravalent cations forming $(MS_4)^{4-}$ (M = Si, Ge, Sn) tetrahedra. Although there are many investigations on the thio-LiSICon Li_4MS_4 electrolytes and the materials derived therefrom, for some of them, the structural details are not clarified in detail yet.

Sensitivity of the structure to processing conditions, subtle changes in stoichiometry and, with respect to analytics, the difficulties due to the weak scattering of lithium, which poses challenges in a detailed understanding of X-ray diffraction patterns, are some of the factors leaving a complex depiction and a wide scope of specific subjects for detailed discussion of the issues on the structure of LiSICon electrolytes. The discussion of the LiSICon structures is grouped into three sections, concerned with (i) results on structure for base materials Li_4SiS_4, Li_4GeS_4 and Li_4SnS_4, (ii) dopants and new Al- and Zn-based LiSICon and (iii) the specific issues related to the structures of Ge- and Si-based phosphosulfides, such as $Li_{4-x}Si_{1-x}P_xS_4$ and $Li_{4-x}Ge_{1-x}P_xS_4$.

4.2.1. *Base materials Li_4SiS_4, Li_4GeS_4 and Li_4SnS_4*

The approaches for an analysis of Li_4SiS_4 and Li_4GeS_4 trace back to the corresponding oxide LiSICon materials Li_4GeO_4, Li_4SiO_4 and Li_3PO_4. The structural works on Li_4SiO_4 agreed that its crystal structure is monoclinic ($P2_1/m$), however, the analysis resulted in differences with respect to ordering *vs.* disordering and the positions of the Li-atoms.[71,72] The outcomes were reconciled with the postulation that Li_4SiO_4 possessed both ordered and disordered arrangements with respect to Li occupancy.[71]

In a powder diffraction study, the Si-based thio-LiSICon material orthorhombic space group *Pnma* with lattice parameters $a = 13.735$ Å, $b = 7.769$ Å, and $c = 6.147$ Å with errors within 0.005 Å was assigned to Li_4SiS_4, synthesized with a high temperature reaction at 1000°C.[3] While the basic building blocks of Li_4SiS_4 consist of isolated $(SiS_4)^{4-}$ tetrahedra surrounded by Li^+ ions like in Li_4SiO_4, the higher symmetry of Li_4SiS_4 compared to Li_4SiO_4 was attributed to the larger ratio of anion radius to cation radius, which induces less distortion of the lattice for Li_4SiS_4. In contrast, for Li_4SiS_4 prepared by a solid-state reaction at 700°C, monoclinic Li_4SiO_4-type structure ($P2_1/m$) with lattice constants a = 6.8934(3)Å, $b = 7.7675(3)$Å, $c = 6.1241(2)$ Å and $\beta = 91.225°$ was reported.[5,31] Li_4GeO_4 is orthorhombic with space group *Cmcm*[73,74] with a transition temperature of ~650°C.[75,76]

Considering Li_4GeS_4, there is agreement that the thio-LiSICon prototype material adopts orthorhombic *Pnma* structure corresponding to the structure of the γ-Li_3PO_4 polymorph. However, there is an open discussion under what specific conditions differing results on the Li-positions in Li_4GeS_4 are realized. The analysis of the diffraction results proposed different arrangements for the Li site in the octahedral voids.

The first report on the structure of Li_4GeS_4 was based on single-crystal X-ray data.[77] The structure was assigned to orthorhombic space group *Pnma* with $(GeS_4)^{4-}$ tetrahedra forming the building blocks of the structure. Three crystallographically independent lithium sites at 8*d*, 4*c* and 8*d*, with two of them having distorted tetrahedral coordination and the third one displaced from the position in the center of the octahedral void, thus being in a square pyramidal arrangement with five sulfur atoms, were identified. Emerging from the displacement, the Li in the octahedral void splits on two crystallographically equivalent sites with an occupancy of 50% each.[77] Rietveld refinements of X-ray data for the structure of polycrystalline Li_4GeS_4 prepared by a solid-state route suggested *Pnma* structure with independent Li-sites at 8*d*, 4*c* and 8*d* and disordered lithium in the octahedral void generating two sites, each 50% occupied, similar to the single crystal result.[4] Combined results from X-ray and neutron powder diffraction data confirmed the space group *Pnma*, but in contrast to the previous results, the Wyckoff positions for the lithium are 8*d*, 4*c* and 4*c*. Moreover, instead of site splitting and disordered lithium in the octahedral void, the refinements indicated an Li-position at the octahedral center.[5] An isostructural solution to the results from the neutron data including agreement on the Li-sites was recently provided for single crystalline Li_4GeS_4.[78]

Two structural modifications, assigned to a low temperature (100 K) and ambient structure, both with space group *Pnma* but with differences in respect of the Li-positions were identified for Li_4SnS_4.[69,78] The differences are in particular related to the octahedral Li-sites. At ambient temperature, the lithium is in tetragonal coordination on Wyckoff positions 4*c* and 8*d*, the lithium in the octahedral void is not disordered, occupying a specific 4*a* position. In contrast, in the low temperature modification, the octahedral coordinated lithium is disordered, occupying two distinct crystallographic sites. Thus, there are of four locations, each with a 25% occupancy.[78] Compared to the ambient temperature modification in the low temperature structure, the cell volume of the latter one is approximately 2% less, mostly due to its smaller *a*-axis lattice parameter. Results from theory however raised the ongoing discussion, if the different Li-substructures are actually due to temperature or if they represent stable (ground-) and metastable states of the material, which emerge from preparation procedures.[79]

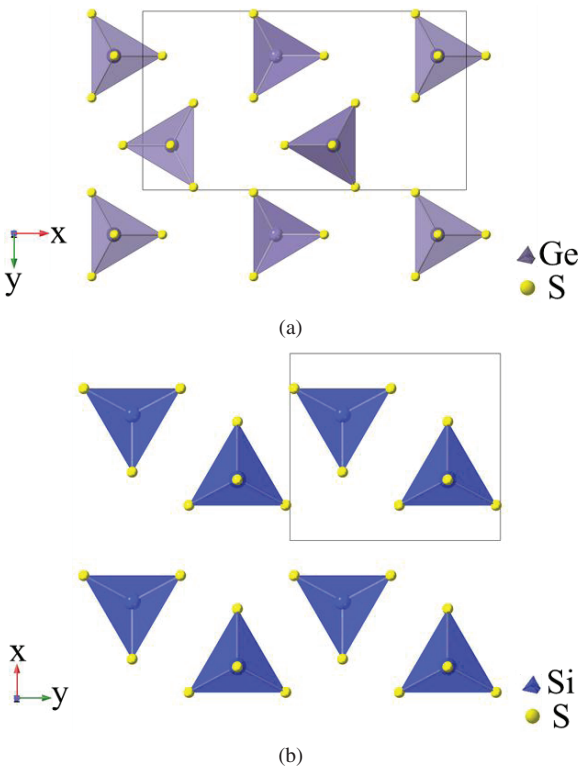

Fig. 19. Arrangement of (a) Li_4GeS_4 drawn from ICSD 95649 and (b) Li_4SiS_4 drawn from ICSD 59708.

A comparison of the lattice parameters and the cell volumes is given in Table 4. The difference between the orientation and packing of $P2_1/m$ and *Pnma* is demonstrated in Fig. 19 with examples from Li_4GeS_4 (*Pnma*) and Li_4SiS_4 ($P2_1/m$).

4.2.2. *Mixed semi/metal systems, dopants and new Zn-based thio-LiSICon*

Modifications of the base materials are aiming to control the conditions for Li-ion conductivity by influencing the lattice spacing, the arrangement of the lithium sites, the occupancy of the lithium positions and the shape of the MS_4 tetrahedra in order to optimize the channels for the Li-transport within the structure. Along with aliovalent doping, structure and lattice volume are influenced not only by the cationic radii but also by the differences in valence and the different amount of

Table 4. Lattice parameters and the cell volumes of base materials.

Material	*a* (Å)	*b* (Å)	*c* (Å)	β (o)	Struc.	References
Li_4SiS_4	6.8934(3)	7.7675(3)	6.1241(2)	91.225(5)	$P2_1/m$	5
Li_4SiS_4 @ 1000°C	13.735	7.769	6.147	90	*Pnma*	3
Li_4GeS_4	14.0340(3)	7.7548(2)	6.15023(17)	90	*Pnma*	80
Li_3PS_4	12.8190(5)	8.2195(4)	6.1236(2)	90	*Pnma*	31
Li_4SnS_4	13.8227(6)	7.9914(3)	6.3913(2)	90	*Pnma*	81

lithium. In many cases, these modifications come along with changes in the structure type. Analyzing the volumes is particularly useful in those cases in which the structure is maintained over the complete range of the solid solution, while in the case of changes, the different structures may provide a basis for the evaluation of correlations to Li-ion conductivity.

Structures of both Li_4GeS_4 and Li_4SnS_4 are orthorhombic with space group *Pnma,* while the tetravalent semi/metal constituents Ge^{4+} and Sn^{4+} form the $(GeS_4)^{4-}$ and $(SnS_4)^{4-}$ backbone. All mixed compositions of $Li_4Ge_{1-x}Sn_xS_4$ are isostructural to the end members of the system. Along with increasing tin content, and along with the increase in ionic radii of Sn^{4+} (0.55 A) *vs.* Ge^{4+} (0.39 A), the lattice parameters ***a***, ***b*** and ***c*** increase up to an Sn-content of $x = 0.8$. The smaller lattice parameter c for the end member Li_4GeS_4 compared to all other $Li_4Ge_{1-x}Sn_xS_4$ materials is attributed to a modified Li-substructure.[81]

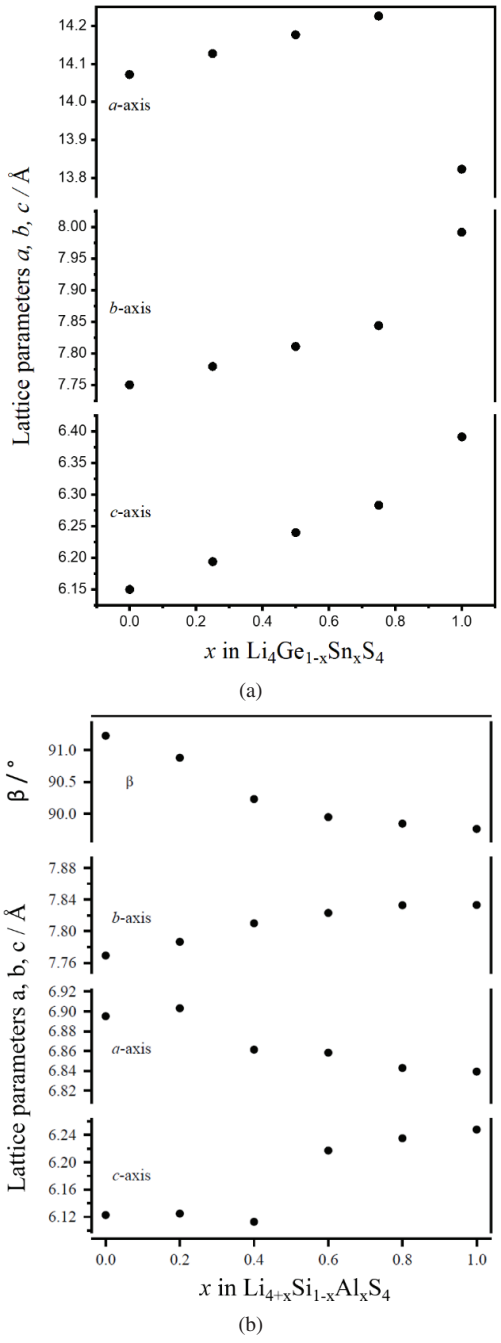

Fig. 20 (a) Lattice parameters of $Li_4Ge_{1-x}Sn_xS_4$ with orthorhombic pace group *Pnma*. Plotted from data in Table S1-S5 of[81] (b) lattice parameters for $Li_{4+x}Si_{1-x}Al_xS_4$ with the monoclinic space group $P2_1/m$. Reprinted with permission from Murayama *et al.* © 2002 Elsevier Science (USA).[5]

The impact of aluminium doping on the structure is different for base materials Li_4SiS_4, *vs.* Li_4GeS_4 and Li_4SnS_4. In case of polycrystalline silicon-based thio-LiSICon, both end members Li_4SiS_4 and Li_5AlS_4 are isostructural with monoclinic space group $P2_1/m$.[5,82] This structural type is maintained within the complete solid solution series $Li_{4+x}Si_{1-x}Al_xS_4$. The lattice constant *a* decreases, whereas *b* and *c* increase with increasing aluminium content (Fig. 20(b)).

In contrast, in the systems $Li_{4+x}Ge_{1-x}Al_xS_4$ and $Li_{4+x}Sn_{1-x}Al_xS_4$, the orthorhombic structures (*Pnma)* of Li_4GeS_4 and Li_4SnS_4 are different from the monoclinic ($P2_1/m$) structure of the aluminium containing analogue Li_5AlS_4. At aluminium contents of $x = 0.4$, solid solutions of Li_4GeS_4–Li_5AlS_4 and Li_4SnS_4–Li_5AlS_4 adopt a structure different from those of both end members, and crystallize in trigonal space group $P\text{-}3m1$.[70] The same type of structural transition from *Pnma* to $P\text{-}3m1$ along with dopant content was detected in the Ga-rich part of the $Li_{4+x}Ge_{1-x}Ga_xS_4$ and $Li_{4+x}Sn_{1-x}Ga_xS_4$ systems, where the electrolytes $Li_{4.4}Ge_{0.6}Ga_{0.4}S_4$ and $Li_{4.4}Sn_{0.6}Ga_{0.4}S_4$ adopt the trigonal structure. Different structures of the end members are also rendered in the Li_4SnS_4–Li_3SbS_4 system.[83] In this system, for electrolytes with $x < 0.5$ of antimony, the orthorhombic *Pnma* structure of Li_4SnS_4 is observed, whereas at antimony dopant contents $x > 0.5$, the material crystallizes in the orthorhombic $Pmn2_1$ space group.[84] Phase mixtures are observed at antimony contents around $x = 0.5$.

The structural description of materials from the $Zn_3(PS_4)_2$–Li_3PS_4 system, which is related to the thio-LiSICon type materials by its Li_3PS_4 end member, is mostly given related to the *bcc* anionic sublattice, in which the zinc and lithium is located in the tetrahedral voids. However, alternatively, the thiophosphate units $(PS_4)^{3-}$ can be considered as the building blocks of the anionic substructure (Fig. 21).[85]

Specifically, in $LiZnPS_4$, all tetrahedral voids in the dense packed $(PS_4)^{3-}$ framework are occupied by lithium or zinc. The structures of the end members Li_3PS_4 and $Zn_3(PS_4)_2$ are orthorhombic (*Pnma*) and tetragonal space group $P\bar{4}n2$. $Li_{1+2x}Zn_{1-x}PS_4$ adopts space group $I\bar{4}$ for materials with $0.125 < x < 0.8$.[86,87]

4.2.3. *Ge- and Si-based phosphosulfides*

Among the Li_4SiS_4 and Li_4GeS_4 based materials, $Li_{4-x}Si_{1-x}P_xS_4$ and $Li_{4-x}Ge_{1-x}P_xS_4$ are, on the one hand, probably the

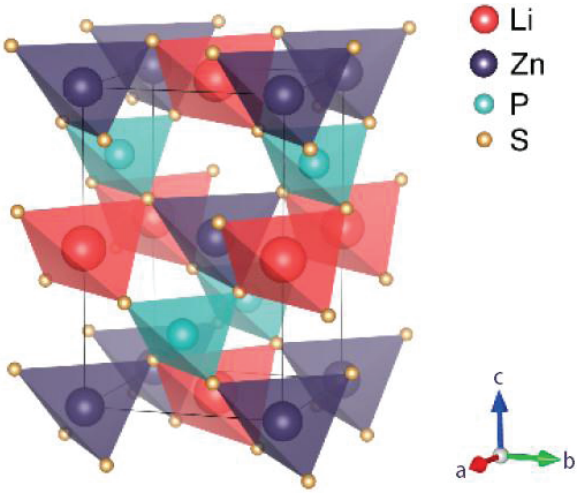

Fig. 21. Structural model of $LiZnPS_4$ emphasizing the PS_4-tetrahedra. Adapted with permission from[86] Copyright © 2018 American Chemical Society.

most interesting electrolytes due to their high Li-ion conductivities. On the other hand, only few confirmed information on the structure of the systems Li_4SiS_4–Li_3PS_4 and Li_4GeS_4–Li_3PS_4 is available.

Within the binary Li_4GeS_4–Li_3PS_4 system, both end members Li_4GeS_4 and Li_3PS_4 are orthorhombic with *Pnma* space group for Li_4GeS_4 and *Pnma* (β-Li_3PS_4) or $Pnm2_1$ (γ-Li_3PS_4) for Li_3PS_4. Initial characterizations of the structures within this system revealed that the structure was not presented over the complete compositional range. While for $Li_{4-x}Ge_{1-x}P_xS_4$ materials with $x < 0.65$ and $x > 0.8$ *Pnma* structured solid solutions were suggested, the structures of $Li_{4-x}Ge_{1-x}P_xS_4$ electrolytes with $0.65 < x < 0.8$ showed additional peaks in the pattern that were attributed to superlattice reflections. Analysis of the structures was addressed by fitting the complete series of materials ($x = 0$, 0.2, 0.4, 0.6, 0.8, 1) using the monoclinic $P2_1/m$ pattern. While for $x < 0.65$ and $x > 0.8$ monoclinic $a \times 3b \times 2c$ type cells were detected, the diffraction patterns indicated $a \times 3b \times 3c$ cells for $Li_{4-x}Ge_{1-x}P_xS_4$ with $0.65 < x < 0.8$. The lattice parameters and the monoclinic angle resulting from this approach are shown in Fig. 22. In contrast to this approach, work on the Li_4GeS_4–Li_3PS_4 phase diagram indicated *Pnma* structure for $Li_{4-x}Ge_{1-x}P_xS_4$ close to Li_4GeS_4 and Li_3PS_4 ($x <$ and $x >$), LGPS-type structure $P4_2/nmc$ for $y < x < z$ and *Pnma*–$P4_2/nmc$ two phase mixtures in the intermediate ranges for x.[88]

In the Li_4SiS_4–Li_3PS_4 system, the structures of the end members, Li_4SiS_4 and Li_3PS_4, are different. Li_4SiS_4 is monoclinic ($P2_1/m$), whereas Li_3PS_4 can be present either in β- or γ-orthorhombic modification (*Pnma* or $Pnm2_1$). The diffraction patterns were indexed to an apparent superlattice of the parent monoclinic Li_4SiS_4 phase using $2a \times 3b \times 2c$ monoclinic ($P2_1/m$) superlattice. In the absence of further details on structural characteristics in the original paper,

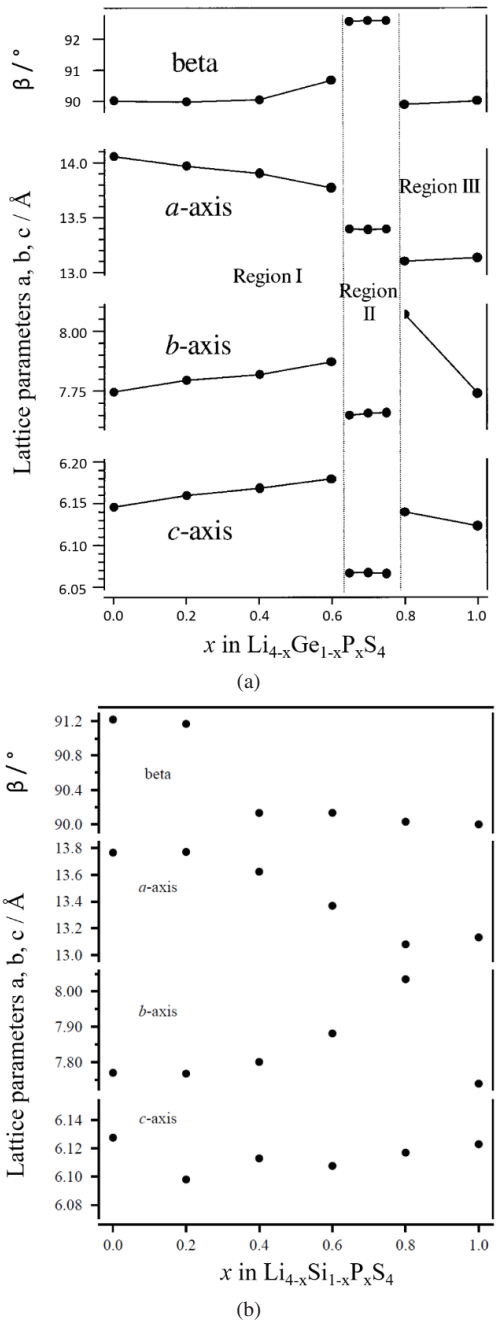

Fig. 22 (a) Lattice parameters for electrolytes in the Li_4GeS_4–Li_3PS_4 system based on Rietveld analysis. Reprinted with permission from Kanno *et al.* © 2001 ECS—The Electrochemical Society.[4] (b) Lattice parameters for electrolytes in the Li_4SiS_4–Li_3PS_4 system for $a \times b \times c$ cells based on fits with a $2a \times 3b \times 2c$ $P2_1/m$ monoclinic superlattice pattern. Reprinted with permission from Murayama *et al.* © 2002 Elsevier Science (USA).[5]

the $Li_{4-x}Si_{1-x}P_xS_4$ lattice parameters for $a \times b \times c$ type cells are shown in Fig. 22(b). In a recent approach, orthorhombic structure (*Pnma*) was identified for $Li_{3.25}Si_{0.25}P_{0.75}S_4$.[89] The arrangement of the lithium, however, is different from the one in the β-Li_3PS_4 lithium substructure. In β-Li_3PS_4, lithium is distributed on two tetrahedral and one octahedral site (Wyckoff positions 8*d*, 4*c* and 4*b*). In contrast, in

$Li_{3.25}Si_{0.25}P_{0.75}S_4$ each of the positions is split into two Li sites, which cannot be occupied within the same cell. Moreover, the lithium in the octahedral site is strongly displaced from the 4*b* position toward an 8*d* site.[89] Though not discussed under the label LiSICon, again different, structures of $Li_{4-x}Si_{1-x}P_xS_4$ materials were detected for electrolytes in the range between $Li_{3.475}Si_{0.475}P_{0.525}S_4$ and $Li_{3.4}Si_{0.4}P_{0.6}S_4$. The space group of these electrolytes was identified to be tetragonal $P4_2/nmc$, similar to the LGPS structure.[90]

4.3. *Thio-LiSICon processing*

Early work on polycrystalline thio-LiSICon was following conventional solid-state route using starting materials Li_2S and semi-metal disulfides GeS_2, SiS_2 for the preparation of Li_4GeS_4 and Li_4SiS_4 base materials.

Common educts for tri- and pentavalent doped thio-LiSICon based on these compounds were Al_2S_3, Ga_2S_3, P_2S_5, respectively. The calcination temperatures for the solid-state processes applied for the synthesis of Li_4GeS_4 and its doped variants were at 600–800°C.[17] Similarly, polycrystalline Li_4SiS_4 was synthesized with educts mixed in a glove-box under argon and heated in a carbon-coated quartz tube at 700°C for 8 h.[5] The same procedure was applied for the preparation of $Li_{4+x}Si_{1-x}Al_xS_4$. An alternative route to obtain Li_4SiS_4 is to homogenize the Li_2S–SiS_2 powder mixture in the liquid state at 1000°C for 1 h first. With melting temperatures of 950°C for Li_2S and 1090°C for SiS_2 the product at 1000°C is in the liquid state. Polycrystalline material is obtained by subsequent annealing of the product at 720°C.[3] Except for the Gallium-doped $Li_{4+x+d}Ge_{1-x-d}Ga_xS_4$ that required excess amounts of lithium, the thio-LiSICon structures were mostly realized with $Li_{4+x}M_{1-x}M'_xS_4$ and $Li_{4-x}M_{1-x}M'_xS_4$ stoichiometric compositions for the materials doped with three- and pentavalent dopants.[17]

Calcination temperatures of 700°C are well below the melting/decomposition temperatures for Li_4GeS_4, Li_4SiS_4 and Li_4SnS_4, which occur in theory at temperatures of 840°C, 1090°C and 865°C, respectively. Experimental work in the form of DTA measurements reproduces the characteristic temperatures only with considerable differences (Fig. 23). In addition to that, the results are very sensitive to impurities such as oxygen contamination.[78] However, for the conditions under which the reaction processes take place, not only the physical conditions of the products but also those of the educts are relevant. Considering the melting points of Li_2S, GeS_2, SiS_2 and SnS_2 at 700°C in theory, all educt components are in the solid state. However, along with slight deviations from ideal stoichiometry, in particular for GeS_2, the solidus temperatures are subject to substantial decrease as evidenced from the phase diagrams (Fig. 24). Consequently, high precision with respect to the stoichiometry of the Li_2S and the

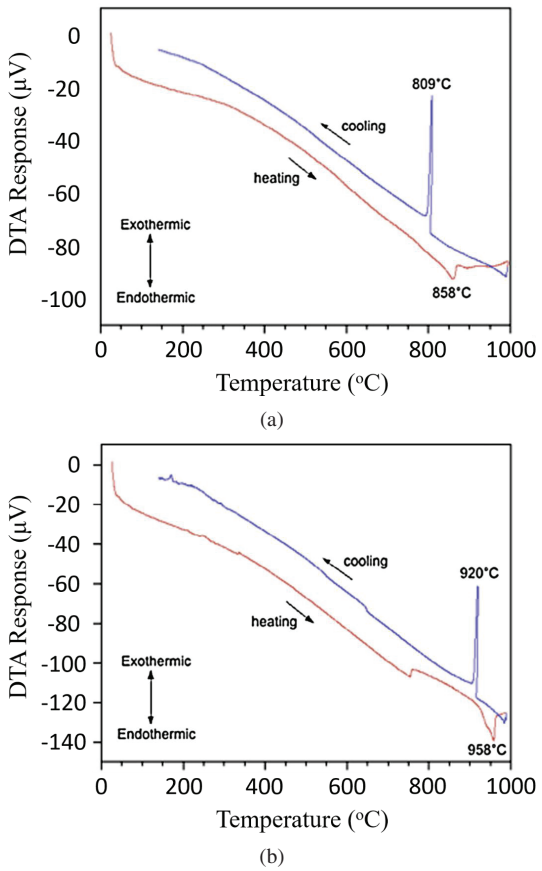

Fig. 23. Results of DTA measurements of (a) Li_4GeS_4 (b) Li_4SnS_4, both heated under carbon-coated, vacuum-sealed fused-silica ampoule. Reprinted with permission from MacNeil *et al.* © 2013 Elsevier B.V.[78]

semi/metal disulfide educts is required to avoid partial formation of liquid phase and to keep the process strictly in a solid-state regime.

While for the thio-LiSICon base compositions Li_4GeS_4, Li_4SiS_4, Li_4SnS_4 temperatures up to 800°C are below the solidus, the addition of dopants may change the physical condition of the reaction products. The DTA curves for $Li_{4-x}Ge_{1-x}P_xS_4$, denoted $(1-k)\ Li_4GeS_4 + k\ Li_3PS_4$ in the original work, indicate that along with increasing phosphorus content, the solidus temperatures are substantially decreasing (Fig. 25).[88] In particular, for materials with $x = 0.67$ and 0.75, $Li_{3.33}Ge_{0.33}P_{0.67}S_4$ and $Li_{3.25}Ge_{0.25}P_{0.75}S_4$, that crystallize in space groups different from *Pnma*, the products are in liquid state when synthesized at 700°C.

In large part of the more recent work, processing temperature conditions at or close to those applied in the early approaches were maintained, even when introducing alternative semi/metal base materials and dopants. Li_4SnS_4,[78] $Li_4Ge_{1-x}Sn_xS_4$[81] and $Li_{4.4}Ge_{0.6-x}Sn_xAl_{0.4}S_4$[70] were prepared by calcination at 750°C for 15 h and at 700 °C for 8 h and 48 h, respectively. Attention has to be paid to impurity contents of the starting materials.[70] Lower calcination temperatures might in some cases be enabled by improved ball milling

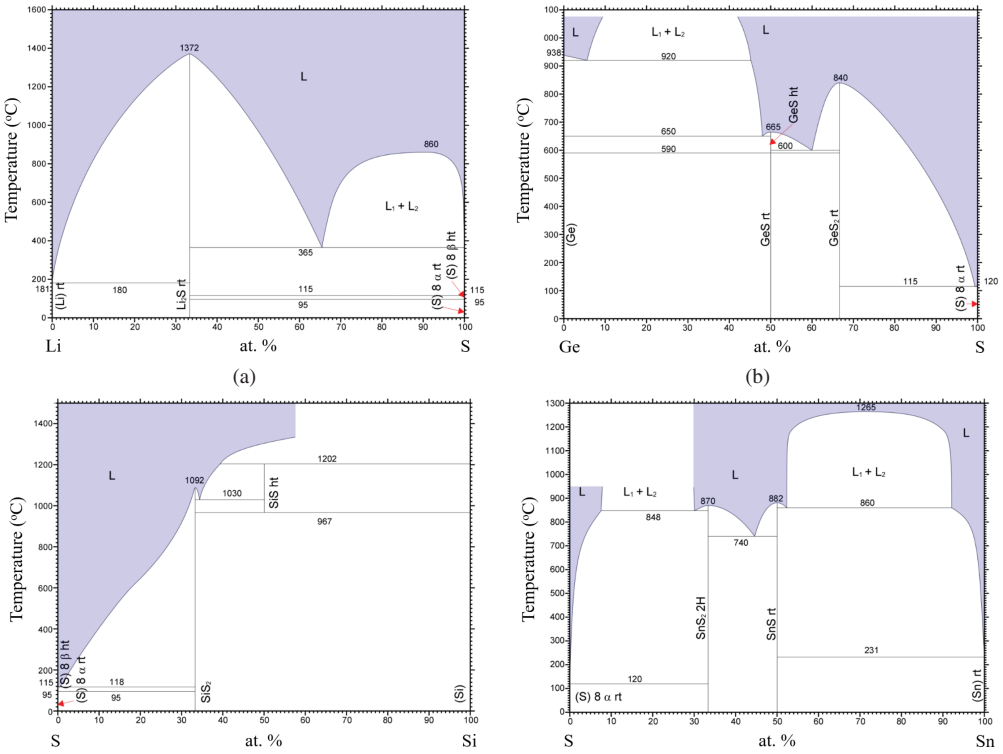

Fig. 24. Binary phase diagrams for the systems (a) Li–S[92] (b) Ge–S[93] (c) S–Si[94] and (d) S–Sn.[95] (Springer-Verlag GmbH, Heidelberg, © 2016).

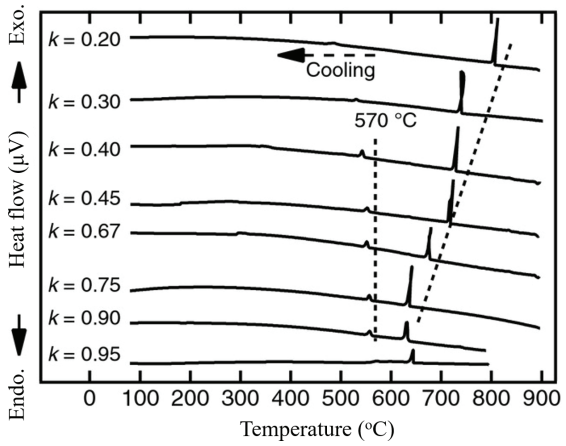

Fig. 25. DTA curves for $Li_{4-x}Ge_{1-x}P_xS_4$, denoted (1-k) Li_4GeS_4 + k Li_3PS_4 in the original figure, recorded on cooling. Reprinted with permission from Hori *et al.* © 2015 The American Ceramic Society.[88]

technology and for tin- and antimony- based thio-LiSICon. Li_4SnS_4[91] and $Li_{4-x}Sn_{1-x}Sb_xS_4$[83] could be synthesized at temperatures as low as 450°C.

A very interesting new approach that uses a liquid phase intermediate, which might improve the homogeneity as well as enable application in industrial scale processing, is a three-step process for the synthesis of Li_4SnS_4.[69] In this approach, the initial product mixture from the high-temperature solid-state reaction was solvent-extracted and recrystallized, then heated under vacuum to remove the co-crystallized solvent.

Specifically, Li_4SnS_4 was prepared by high-temperature reactions of lithium sulfide, tin, and sulfur, with unreacted starting material and polysulfide by-product being present in non-negligible amounts. The second step included the generation of the hydrate $Li_4SnS_4 \cdot 13H_2O$, which was obtained by extraction with water, followed by filtration and ensuing slow evaporation of the solvent. In the third consecutive step, dehydration of the solution by heating to 320 °C under 10^{-6} Pa for 4 h to the polycrystalline phase was obtained. Thus, anhydrous Li_4SnS_4 can be produced from its hydrated form through direct dehydration without hydrolysis and oxidation from air. Li_4SnS_4 was also synthesized by mechanical milling at 510 rpm for 40 h, however, in contrast to the thermal processes, this process yields Li_4SnS_4 in hexagonal $P6_3/mmc$ phase.[96]

In order to produce X-ray high-quality single crystals, flux methods proved more effective. For preparation of Li_4GeS_4, single crystals with crystal size up to about $7 \times 6 \times 2$ mm^3; Li_2S, GeS_2 and S in a 4:1:4 mole ratio were mixed, ground and heated in an evacuated carbon-coated fused silica tube at 10^{-5} Torr to 400°C for 12 h, to 750°C for 200 h, then slowly cooled to 500°C followed by quenching to ambient temperature. The product was isolated with MeOH.[77]

4.4. *Thio-LiSICon type conductivity*

Analysis of the Li-ion conductivities of the thio-LiSICon electrolytes focuses on two different aspects of the development

of this type of materials. First, the effects of the polarization approach and the dopant strategies on Li-ion conductivity are pointed out for the most important and well established Ge- and Si-based thio-LiSICon based electrolytes. Second, a discussion of more recent work on thio-LiSICon electrolytes encompassing sulfide Li-ion conductors of the Li_4MX_4 and $Li_4M'_{1-x}M''_xX_4$ type with extended scope of semi/metals base materials and dopants will be taken up. More elaborate processing procedures of these recent developments render the direct comparison to the conventional LiSICon materials difficult.

4.4.1. *Ge-based thio-LiSICon*

The compound analysis of the conductivities of the thio-LiSICon materials reflects the efficiency of both the polarization approach and the dopant strategies of Ge- and Si-based materials (Fig. 26). The Li-ion conductivity of the oxide-based LiSICon electrolyte Li_4GeO_4 is ~ 2.5×10^{-10} S cm^{-1} at 100°C (red).[76] Replacement of the oxygen anion by high-polarizing sulfur increases the ambient temperature Li-ion conductivities by several orders of magnitude to 2×10^{-7} S cm^{-1} for Li_4GeS_4.[17]

In the Ge-based electrolytes, pronounced differences of the impact of the different dopant strategies are demonstrated. Li-vacancy doping by Zn^{2+} substitution for two Li^+ shows only slight impact on the ambient temperature Li-ion conductivities, which give the highest values of 3×10^{-7} S cm^{-1} for electrolytes from the $Li_{4-2x}Zn_xGeS_4$ series (at x = 0.05).[17] In contrast, generating Li-interstitials by substituting part of the Ge^{4+} by Ga^{3+} or Sb^{3+} along with concomitant adjustment of the Li-content according to $Li_{4+x}Ge_{1-x}Ga_xS_4$ results in an improvement in Li-ion conductivity of more than two orders of magnitude. A maximum ambient temperature Li-ion conductivity of $\sigma = 4.4 \times 10^{-6}$ S cm^{-1} is reported for $Li_{4-x}Ge_{1-x}Sb_xS_4$.[22] The highest ambient temperature Li-ion conductivity among the Ga^{3+} doped group is achieved in $Li_{4.25}Ge_{0.75}Ga_{0.25}S_4$ with 6.5×10^{-5} S cm^{-1}.[17]

The impact of the phosphorus doping has to be considered differentiating between electrolyte materials for which the structure is left along with *Pmn*2$_1$ (γ-Li_3PO_4) or *Pnma* (β-Li_3PO_4) space group and those that initiate structural changes with respect to the space group (full *vs.* open blue symbols in Fig. 26). While the impact on the Li-ion conductivity of the former is similar than for the Ga and Sb doping approach, the combined effects of P-doping and structural changes provide extremely high conductivities, most pronounced for the $Li_{3.25}Ge_{0.25}P_{0.75}S_4$, for which the ambient temperature Li-ion conductivity amounts to 2.2×10^{-3} S cm^{-1}. However, along with the changes in structure, these materials although historically referred to as thio-LiSICon, are not thio-LiSICon according to a definition given by the structure.

4.4.2. *Si-based thio-LiSICon*

The Li-ion conductivity of oxide LiSICon electrolyte based on Si (Fig. 27) is ~ 2.5×10^{-9} S cm^{-1} at 100°C, thus higher than that of Li_4GeO_4 (red).[76] The oxygen to sulfur exchange approach increases the ambient temperature Li-ion conductivity by more than an order of magnitude to 5×10^{-8} S cm^{-1} for Li_4SiS_4.[3,97] Doping with interstitials by substituting part of the Si^{4+} by Al^{3+} according to $Li_{4+x}Si_{1-x}Al_xS_4$ results only in slight improvement in Li-ion conductivity for most of

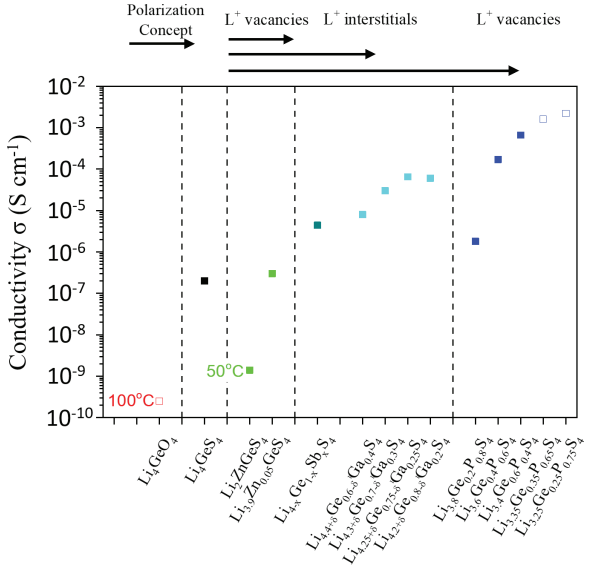

Fig. 26. Li-ion conductivities of Ge-based thio-LiSICon electrolytes. Conductivities for all thio-LiSICon materials are at ambient temperature unless otherwise indicated. Data and references can be found in Table 5.

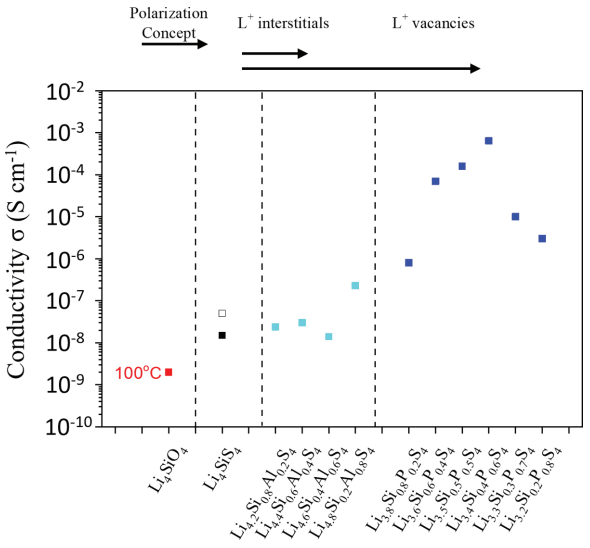

Fig. 27. Li-ion conductivities of Si-based thio-LiSICon electrolytes. Conductivities for all thio-LiSICon materials are at ambient temperature unless otherwise indicated. Data and references can be found in Table 5.

the compositions. An increase of the ambient temperature Li-ion conductivity to $\sigma = 2.3 \times 10^{-7}$ S cm^{-1} is reported for $Li_{4.8}Si_{0.2}Al_{0.8}S_4$.[5] In the Si-based thio-LiSICon, an increase to ambient temperature Li-ion conductivities higher than 2×10^{-4} S cm^{-1} can be realized by phosphorus-doping induced creation of Li-vacancies. The conductivities amount up $\sigma = 1.5 \times 10^{-4}$ S cm^{-1} and 7×10^{-4} S cm^{-1} for $Li_{3.5}Si_{0.5}P_{0.5}S_4$ and $Li_{3.4}Si_{0.4}P_{0.6}S_4$ electrolytes, respectively. However, also for this group of materials, their structure and thus the attribution to the thio-LiSICon type is still under discussion.

4.4.3. *Ge-based versus Si-based thio-LiSICon*

The developments of the Li-ion conductivity for the established Ge- and Si-based systems along with the dopant strategies follow qualitatively the same pattern, but are quantitatively different (Fig. 28). The ambient temperature Li-ion conductivities of Li_4SiS_4 and Li_4GeS_4 are 10^{-8} to 10^{-7} S cm^{-1} thus in a range within one order of magnitude. Modifying the base materials according to an interstitial doping approach with M^{3+} based thio-LiSICon materials is arranged by substituting tetravalent Ge^{4+} or Si^{4+} by trivalent Ga^{3+} or Al^{3+}. Li-ion electrolytes based on both dopants metals, Li_5AlS_4 and Li_5GaS_4, have substantial lower Li-ion conductivities than the base materials (1.5×10^{-9} S cm^{-1} for Li_5AlS_4 (at 100°C) and 5.1×10^{-8} S cm^{-1} for Li_5GaS_4 (at 100°C)).[17,97] Nevertheless, doping results in an increase of Li-ion conductivity for the solid solutions, which is moderate for $Li_{4+x}Si_{1-x}Al_xS_4$ and quite pronounced for $Li_{4+x}Ge_{1-x}Ga_xS_4$. Applying vacancy doping, the conductivity of the phosphorus-based dopant component Li_3PS_4, for which the conductivity is significantly higher than those of the base materials, provides an enhanced ambient temperature Li-ion conductivity for the phosphorus-doped Si- and Ge-based materials to 10^{-6} or 10^{-4} S cm^{-1}, respectively, for those materials that maintain the orthorhombic thio-LiSICon structure. In part of the $Li_{4-x}M_{1-x}P_xS_4$ (M = Ge, Si) electrolytes, the phosphorus doping leads to a change in structure, which results in considerable increase of the ambient temperature Li-ion conductivities to 8×10^{-3} and 2×10^{-2} S cm^{-1} for Si- and Ge-based materials, respectively.

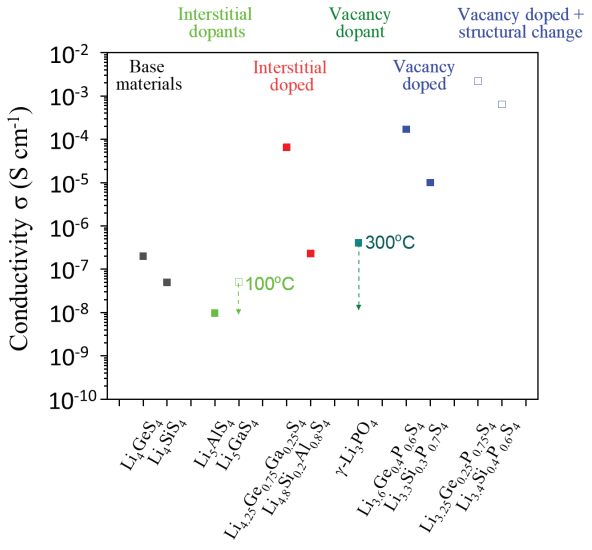

Fig. 28. Li-ion conductivities for germanium- and silicon-based thio-LiSICon electrolytes compared for the base compositions and the "best of" materials, dopants and doped materials for interstitial and vacancy doping. Conductivities for all the thio-LiSICon materials are at ambient temperature unless otherwise indicated. Data and references can be found in Table 5.

4.5. *Recent developments of thio-LiSICon electrolytes*

While thio-LiSICon electrolytes based on Si and Ge are well established, recent approaches tend to investigate materials with different base metal and semi-metal components. These developments of the thio-LiSICon type of materials encompass investigations of aluminium-based phosphosulfide electrolytes, electrolytes of the Li_4MX_4 and $Li_4M'_{1-x}M''_xX_4$ types containing zinc and tin-based thio-LiSICon Li_4SnS_4 with interstitial doping approaches applied to Li_4GeS_4 and Li_4SnS_4 by using aluminium as the dopant.

An ambient temperature Li-ion conductivity of 8.02×10^{-4} S cm^{-1} was measured for the Al-based electrolyte $Li_{3.667}Al_{0.333}P_{0.667}S_4$, denoted as $Li_{11}AlP_2S_{12}$ in the original paper.[98] The structure of the material is however not orthorhombic, but corresponds to the structure found in $Li_{4-x}Ge_{1-x}P_xS_4$ for $0.65 < x < 0.8$.[4] Compared to the Li_5AlS_4 base material with monoclinic $P2_1/m$ structure,[80] for which Li-ion conductivities of 1.5×10^{-9} S cm^{-1},[5] and 9.7×10^{-9} S cm^{-1} at 50°C were reported,[82] the doping with phosphorus improves the Li-ion conductivity by almost five orders of magnitude.

Zn-based $Li_{1+2x}Zn_{1-x}PS_4$ type electrolytes are related to the thio-LiSICon type materials by their $LiZnPS_4$–Li_3PS_4 origin. Conductivities within the series $Li_{1+2x}Zn_{1-x}PS_4$ (x = 0.125, 0.25, 0.375, 0.5, 0.625, 0.75, 0.8, 0.9)[87] and (x = 0.25, 0.5, 0.75)[86] range from 10^{-8} S cm^{-1} to more than 10^{-4} S cm^{-1} at ambient temperature. The ambient temperature Li-ion conductivity for the $I\bar{4}$ structured $LiZnPS_4$ end member is 1.81×10^{-12} S cm^{-1}.[99] Maximum ambient temperature Li-ion conductivities within these series were found for 5.7×10^{-4} S cm^{-1} at $x = 0.625$ and 8.40×10^{-4} S cm^{-1} at $x = 0.75$, respectively.[86,87]

Most extensive developments among the recent investigations of the thio-LiSICon type of materials are related to tin-based Li_4SnS_4 type electrolytes and modifications thereof.[69] The *Pnma* structured tetralithium *ortho*-sulfidostannate has an Li-ion conductivity as high as 7×10^{-5} S cm^{-1} at 20°C, thus being almost three orders of magnitude higher than for Li_4SiS_4 or Li_4GeS_4. Even higher Li-ion conductivity, which amounts to 1.1×10^{-4} S/cm, was found for the $P6_3/mmc$ non-thio-LiSICon

Li_4SnS_4 polymorph. Synthesizing solid solutions of Li_4SnS_4 and Li_4GeS_4, however, does not improve Li-ion conductivities.[81] Up to a Ge-content of $x = 0.75$, the ambient temperature Li-ion conductivity in $Li_4Sn_{1-x}Ge_xS_4$ is approximately one order of magnitude less than for Li_4SnS_4, for which $\sigma = 1.4 \times 10^{-6}$ S cm^{-1} was measured in this study.[81] Dopant-modified electrolytes of the stannate material were focusing on the vacancy dopant approach employing pentavalent cations replacing Sn^{4+} concomitant with reduction in Li-content. The doping with arsenic results in further improvement of the ambient temperature Li-ion conductivity amounting to 1.39×10^{-3} S cm^{-1}.[100] $Li_{4-x}Sb_xSn_{1-x}S_4$ solid solutions ($0 < x < 0.5$), as non-toxic alternatives to the As-doped stannate, provide comparatively lower, but still very high Li-ion conductivity. In particular, for the $Li_{3.8}Sb_{0.2}Sn_{0.8}S_4$ electrolyte with good air stability[78] and negligible trend to the formation of

Table 5. Li-ion conductivity and activation energies of LiSICon structures at ambient temperature unless otherwise stated.

Stoichiometry	Crystal system	σ (S cm^{-1})	E_a (eV)	References
Li_4SiO_4	$P2_1/m$	2.5×10^{-9} (100°C)	0.78	76
Li_4GeO_4	—	2.5×10^{-10} (100°C)	0.90	76
γ-Li_3PO_4	Orthorhombic	4.1×10^{-7} (300°C)	1.14	101
Li_4GeS_4	Orthorhombic	2.0×10^{-7}	—	17
Li_2GeS_3	Orthorhombic	9.7×10^{-9} (125°C)	—	17
Li_2GeZnS_4	Orthorhombic	1.4×10^{-9} (50°C)	—	17
$Li_{3.9}GeZn_{0.005}S_4$	Orthorhombic	3.0×10^{-7}	—	17
$Li_{4-x}Ge_{1-x}Sb_xS_4$	—	4.4×10^{-6}	—	22
$Li_{4.2+\delta}Ge_{0.8-\delta}{}^{I}Ga_{0.2}S_4$	Orthorhombic	6.0×10^{-5}	0.35	17
$Li_{4.25+\delta}Ge_{0.75-\delta}{}^{I}Ga_{0.25}S_4$	Orthorhombic	6.5×10^{-5}	0.33	17
$Li_{4.3+\delta}Ge_{0.7-\delta}{}^{I}Ga_{0.3}S_4$	Orthorhombic	3.0×10^{-5}	0.35	17
$Li_{4.4+\delta}Ge_{0.6-\delta}{}^{I}Ga_{0.4}S_4$	Orthorhombic	8.0×10^{-6}	0.39	17
$Li_{3.25}Ge_{0.25}P_{0.75}S_4$	$P2_1/m$	2.2×10^{-3}	0.20	4
$Li_{3.35}Ge_{0.35}P_{0.65}S_4$	$P2_1/m$	1.6×10^{-3}	0.23	4
$Li_{3.4}Ge_{0.6}P_{0.4}S_4$	$P2_1/m$	6.6×10^{-4}	0.27	4
$Li_{3.6}Ge_{0.4}P_{0.6}S_4$	$P2_1/m$	1.7×10^{-4}	0.34	4
$Li_{3.8}Ge_{0.2}P_{0.8}S_4$	$P2_1/m$	1.8×10^{-6}	0.47	4
Li_4SiS_4	$Pnma$	5.0×10^{-8}	0.60	3
Li_4SiS_4	$P2_1/m$	1.5×10^{-8}	-	5
$Li_{3.2}Si_{0.2}P_{0.8}S_4$	$P2_1/m$	3.0×10^{-6}	0.37	5
$Li_{3.3}Si_{0.3}P_{0.7}S_4$	$P2_1/m$	1.0×10^{-5}	0.36	5
$Li_{3.4}Si_{0.4}P_{0.6}S_4$	$P2_1/m$	6.4×10^{-4}	0.29	5
$Li_{3.5}Si_{0.5}P_{0.5}S_4$	$P2_1/m$	1.6×10^{-4}	0.34	5
$Li_{3.6}Si_{0.6}P_{0.4}S_4$	$P2_1/m$	7.0×10^{-5}	0.35	5
$Li_{3.8}Si_{0.8}P_{0.2}S_4$	$P2_1/m$	8.0×10^{-7}	0.37	5
Li_5AlS_4	$P2_1/m$	9.7×10^{-9}	0.61	82
Li_5AlS_4	$P2_1/m$	1.5×10^{-9}	-	5
$Li_{4.8}Si_{0.2}Al_{0.8}S_4$	$P2_1/m$	2.3×10^{-7}	0.52	5
$Li_{4.6}Si_{0.4}Al_{0.6}S_4$	$P2_1/m$	1.4×10^{-8}	0.525	5
$Li_{4.4}Si_{0.6}Al_{0.4}S_4$	$P2_1/m$	3.0×10^{-8}	0.525	5
$Li_{4.2}Si_{0.8}Al_{0.2}S_4$	$P2_1/m$	2.4×10^{-8}	0.53	5
$Li_{4.4}Al_{0.4}Sn_{0.6}S_4$	P-3m1	4.3×10^{-6}	0.42	70
$Li_{4.4}Al_{0.4}Ge_{0.6}S_4$	P-3m1	4.3×10^{-5}	0.38	70
$Li_{2.5}Zn_{0.25}PS_4$	$I\bar{4}$	8.4×10^{-4}	—	86
$Li_{2.25}Zn_{0.375}PS_4$	$I\bar{4}$	5.7×10^{-4}	0.35	87
$Li_{3.9}GeZn_{0.05}S_4$	Orthorhombic	3.0×10^{-7}	0.52	17
$Li_{3.25}Ge_{0.25}P_{0.75}S_4$	$P2_1/m$	2.2×10^{-3}	0.207	4
$Li_{3.25}Ge_{0.25}P_{0.75}S_4$	-	1.82×10^{-4} (30°C)	0.42	102
Li_5GaS_4	Orthorhombic	5.1×10^{-8} (100°C)	–	17
Li_4SnS_4	$Pnma$	7×10^{-5} (20°C)	0.41	69
$Li_{3.8}Sb_{0.2}Sn_{0.8}S_4$	$Pnma$	3.5×10^{-4}	0.197	83

H_2S in contact with humid air, $\sigma = 3.5 \times 10^{-4}$ S cm^{-1} was measured at ambient temperature.[83] Materials based on Li, Sn, S including phosphorus adopt *P*42*/nmc* LGPS structure.

Both, Li_4GeS_4 and Li_4SnS_4 within the systems Li_4GeS_4–Li_5AlS_4 and Li_4SnS_4–Li_5AlS_4, were subject to recent investigations on the impact of interstitial lithium by aluminium doping within the systems Li_4GeS_4–Li_5AlS_4 and Li_4SnS_4–Li_5AlS_4. While hitherto Ga and Sb had been under consideration as interstitial dopants in Ge-based thio-LiSICon,[4] the new combinations Ge–Al and Sn–Al resulted in innovative electrolytes with trigonal structure *P*–3*m*1 for $X = 0.4$. The ambient temperature Li-ion conductivity of the $Li_{4.4}Al_{0.4}Sn_{0.6}S_4$ electrolyte is 4.3×10^{-6} S cm^{-1}. In $Li_{4.4}Al_{0.4}Ge_{0.6}S_4$ with the same structure, the conductivity amounts to 4.3×10^{-5} S cm^{-1}, thus being one order of magnitude higher than for its Sn-based counterpart.[70]

A summary of the Li-ion conductivities of the LiSICon type electrolytes including the information of the structure is given in Table 5.

5. Conclusion

This part I of the review on phosphosulfide electrolytes started by giving the application background for the development of Li-ion conductive solid-state electrolytes and provides a brief overview on the four types of phosphosulfide electrolytes under discussion for designing all-solid-state Li-ion batteries with metallic lithium anodes. Thereby, Li–P–S, LiSICon, LGPS and Argyrodite-type electrolytes were distinguished. Two of them, the Li–P–S type and the LiSICon type electrolytes were subject to detailed descriptions over a wide variety of compositions in part I.

First, the chemistry of the materials in the context of Li–P–S and Li_2S–P_2S_5–MS_S phase diagrams was considered. Subsequently the phosphosulfide electrolytes within both the types were analyzed considering their structural characteristics, the options for the processing and compared with respect to their Li-ion conductivities at ambient temperature. In both the types, electrolytes with high Li-ion conductivities were identified. It is pointed out, that the Li-ion conductivity does not exclusively depend on the chemical compositions, but is also crucially influenced by the processing routes and the sample preparation procedures, which result in differences with respect to the interface contacts between grains or particles in the electrolyte.

The treatise will be continued in part II of this review, in which first the more recently developed types of phosphosulfide electrolytes, the LGPS type and the Argyrodite type, will be discussed following the same concepts as for Li–P–S type and LiSICon type in part I. Before turning to the perspective of research on the phosphosulfide electrolytes there, two most essential issues, the Li-ion conductivity and the electrochemical stability *vs.* metallic lithium will be examined in an inter type comparison of selected materials from each type.

Acknowledgment

Support of the work by the project "High Performance Solid-State Batteries" (HIPSTER) from "Ministerium für Kultur und Wissenschaft des Landes Nordrhein-Westfalen" is gratefully acknowledged.

References

1. M. V. Reddy *et al.*, *Materials* **13**, 1884 (2020).
2. R. Schmuch *et al.*, *Nat Energy* **3**, 267 (2018).
3. B. T. Ahn and R. A. Huggins, *Mater. Res. Bull.* **24**, 889 (1989).
4. R. Kanno and M. Maruyama, *J. Electrochem. Soc.* **148**, 742 (2001).
5. M. Murayama *et al.*, *J. Solid State Chem.* **168**, 140 (2002).
6. H. J. Deiseroth *et al.*, *Angew. Chem. Int. Edit.* **47**, 755 (2008).
7. N. Kamaya *et al.*, *Nat. Mater.* **10**, 682 (2011).
8. Y. Wang *et al.*, *Nat. Mater*. **14**, 1026 (2015).
9. X. T. Bai *et al.*, *J. Mater. Chem. A* **8**, 25663 (2020).
10. M. Ghidiu *et al.*, *J. Mater. Chem. A* **7**, 17735 (2019).
11. Y. Kato *et al.*, *Adv. Energy Mater.* **10**, 2002153 (2020).
12. O. U. Kudu *et al.*, *J. Power Sources* **407**, 31 (2018).
13. A. Miura *et al.*, *Nat. Rev. Chem*. **3**, 189 (2019).
14. K. H. Park *et al.*, *Adv. Energy Mater.* **8**, 1800035 (2018).
15. Y. Nikodimos *et al.*, *Energ Environ. Sci.* **15**, 991–1033 (2022).
16. T. Krauskopf *et al.*, *Chem. Rev.* **120**, 7745–7794 (2020).
17. R. Kanno *et al.*, *Solid State Ionics* **130**, 97 (2000).
18. A. W. Eissenbach, *Neues Jahrb. Geol. Paläontol* **2**, 67 (1886).
19. S. Adams and R. P. Rao, *J. Mater. Chem.* **22**, 7687 (2012).
20. H. Eckert *et al.*, *Chem. Mater*. **2**, 273 (1990).
21. M. Tatsumisago *et al.*, *Solid State Ionics* **154**, 635 (2002).
22. M. Murayama *et al.*, *Solid State Ionics* **170**, 173 (2004).
23. R. Mercier *et al.*, *J. Solid State Chem.* **43**, 151 (1982).
24. C. Dietrich *et al.*, *Chem. Mater*. **28**, 8764 (2016).
25. D. Y. Oh *et al.*, *Chemsuschem* **13**, 146 (2020).
26. Z. Lin *et al.*, *Angew. Chem. Int. Edit.* **52**, 7460 (2013).
27. Y. Kato *et al.*, *Nat. Energy* **1**, 16030 (2016).
28. C. Dietrich *et al.*, *Inorg. Chem*. **56**, 6681 (2017).
29. H. Yamane *et al.*, *Solid State Ionics* **178**, 1163 (2007).
30. S. Ito *et al.*, *J. Power Sources* **271**, 342 (2014).
31. K. Homma *et al.*, *Solid State Ionics* **182**, 53 (2011).
32. K. Homma *et al.*, *J. Phys. Soc. Jpn*. **79**, 90 (2010).
33. K. Kaup *et al.*, *J. Mater. Chem. A* **8**, 12446 (2020).
34. S. T. Kong *et al.*, *Chem.-Eur. J*. **16**, 5138 (2010).
35. F. Zheng *et al.*, *J. Power Sources* **389**, 198–213 (2018).
36. X. Lu *et al.*, *Electrochem. Sci. Adv.* e2100208 (2022).
37. T. A. Yersak *et al.*, *Front Energy Res*. **10**, 882508 (2022).
38. A. Hayashi *et al.*, *J. Mater. Chem. A* **1**, 6320–6326 (2013).
39. Y. T. Chen *et al.*, *J. Mater. Chem. A* **10**, 7155–7164 (2022).
40. J. R. Xu *et al.*, *Adv. Energy Mater.* **12**, 2200244 (2022).
41. J. Schnell *et al.*, *J. Power Sources* **382**, 160–175 (2018).
42. Y. J. Nam *et al.*, *J. Power Sources* **375**, 93–101 (2018).
43. K. Lee *et al.*, *Acs Energy Lett.* **4**, 1918–1929 (2019).
44. M. Tachez *et al.*, *Solid State Ionics* **14**, 181 (1984).

45. R. Garcia-Mendez *et al.*, *Electrochim. Acta* **237**, 144 (2017).
46. Z. C. Liu *et al.*, *J. Am. Chem. Soc.* **135**, 975 (2013).
47. H. Wang *et al.*, *J. Mater. Chem. A.* **4**, 8091 (2016).
48. N. H. H. Phuc *et al.*, *Solid State Ionics*, **288**, 240 (2016).
49. M. Duchardt *et al.*, *Acs Appl. Energ. Mater*. **3**, 6937 (2020).
50. J. F. Brice, *Cr. Acad. Sci. C Chim*. **283**, 581 (1976).
51. D. A. Ziolkowska *et al.*, *Acs Appl. Mater. Inter*. **11**, 6015 (2019).
52. Z. D. Hood *et al.*, *Solid State Ionics* **284**, 61 (2016).
53. I. H. Chu *et al.*, *Acs Appl. Mater. Inter.* **8**, 7843 (2016).
54. Y. Seino *et al.*, *Energ Environ. Sci.* **7**, 627 (2014).
55. M. R. Busche *et al.*, *Chem. Mater*. **28**, 6152 (2016).
56. F. Mizuno *et al.*, *Solid State Ionics* **177**, 2721 (2006).
57. K. Minami *et al.*, *Solid State Ionics* **178**, 837 (2007).
58. M. Calpa *et al.*, *RSC Adv*. **7**, 46499 (2017).
59. R. C. Xu *et al.*, *Electrochim. Acta* **219**, 235 (2016).
60. Y. X. Wang *et al.*, *Chem. Mater*. **30**, 990 (2018).
61. C. Dietrich *et al.*, *J. Mater. Chem. A.* **5**, 18111 (2017).
62. F. Marchini *et al.*, *Adv. Energy Mater.* **11**, 2101111 (2021).
63. A. Hayashi *et al.*, *Electrochem. Commun*. **5**, 111 (2003).
64. H. J. Deiseroth *et al.*, *Z. Anorg. Allg. Chem*. **637**, 1287 (2011).
65. M. Tatsumisago *et al.*, *J. Power Sources* **159**, 193 (2006).
66. K. Minami *et al.*, *J. Ceram. Soc. Jpn*. **118**, 305 (2010).
67. X. Y. Yao *et al.*, *Nano Lett*. **16**, 7148 (2016).
68. B. Xue *et al.*, *J. Am. Ceram. Soc*. **102**, 3402 (2019).
69. T. Kaib *et al.*, *Chem. Mater*. **24**, 2211 (2012).
70. B. T. Leube *et al.*, *Chem. Mater*. **30**, 7183 (2018).
71. D. Tranqui *et al.*, *Acta Crystallograp. B-Struct. Sci.* **35**, 2479 (1979).
72. A. W. H. Völlenkle and H. Nowotny, *Chemical Monthly* **99**, 1360 (1968).
73. R. Hofmann and R. Hoppe, *Z. Anorg. Allg. Chem*. **555**, 118 (1987).
74. H. Vollenkle and A. Wittmann, *Z. Kristallogr. Krist*. **128**, 66 (1969).
75. P. G. Bruce and A. R. West, *Mater. Res. Bull.* **15**, 379 (1980).
76. I. M. Hodge *et al.*, *J. Am. Ceram. Soc*. **59**, 360 (1976).
77. Y. Matsushita and M. G. Kanatzidis, *Z. Naturforsch. B* **53**, 23 (1998).
78. J. H. MacNeil *et al.*, *J. Alloy. Compd*. **586**, 736 (2014).
79. A. Al-Qawasmeh *et al.*, *J. Electrochem. Soc.* **164**, 6386 (2017).
80. M. Murayama *et al.*, *Solid State Ionics* **154**, 789 (2002).
81. N. Minafra *et al.*, *Chem. Mater.* **31**, 3794 (2019).
82. H. Lim *et al.*, *J. Solid State Chem.* **257**, 19 (2018).
83. Z. R. Zhang *et al.*, *J. Energy Chem*. **41**, 171 (2020).
84. K. H. Kim and S. W. Martin, *Chem. Mater*. **31**, 3984 (2019).
85. J. Stefan *et al.*, *Z. Anorg. Allg. Chem*. **628**, 1765 (2002).
86. K. Kaup *et al.*, *Chem. Mater*. **30**, 592 (2018).
87. N. Suzuki *et al.*, *Chem. Mater*. **30**, 2236 (2018).
88. S. Hori *et al.*, *J. Am. Ceram. Soc*. **98**, 3352 (2015).
89. L. D. Zhou *et al.*, *Chem. Mater*. **31**, 7801 (2019).
90. S. Hori *et al.*, *Faraday Discuss.* **176**, 83 (2014).
91. G. Sahu *et al.*, *Energ. Environ. Sci.* **7**, 1053 (2014).
92. P. Villars and H. Okamoto, Li-S Binary Phase Diagram 0-100 at.% S: Datasheet from "PAULING FILE Multinaries Edition — 2012" in SpringerMaterials (https://materials.springer.com/isp/phase-diagram/docs/c_0100210) (Springer-Verlag, Berlin).
93. P. Villars and H. Okamoto, Ge-S Binary Phase Diagram 0-100 at.% S: Datasheet from "PAULING FILE Multinaries Edition – 2012" in SpringerMaterials (https://materials.springer.com/isp/phase-diagram/docs/c_0901214), (Springer, Berlin).
94. S. P. Villars and H. Okamoto, -Si Binary Phase Diagram 0-100 at.% Si: Datasheet from "PAULING FILE Multinaries Edition – 2012" in SpringerMaterials (https://materials.springer.com/isp/phase-diagram/docs/c_0101219), (Springer, Berlin).
95. P. Villars and H. Okamoto, S-Sn Binary Phase Diagram 0-100 at.% Sn: Datasheet from "PAULING FILE Multinaries Edition — 2012" in SpringerMaterials (https://materials.springer.com/isp/phase-diagram/docs/c_0903413), (Springer-Verlag, Berlin).
96. K. Kanazawa *et al.*, *Inorg. Chem*. **57**, 9925 (2018).
97. R. Kanno *et al.*, *Solid State Ionics: Trends in the New Millennium, Proceedings* (2002), pp. 13–22. https://doi.org/10.1142/9789812776259_0003
98. P. F. Zhou *et al.*, *Chem. Commun*. **52**, 6091 (2016).
99. W. D. Richards *et al.*, *Energ. Environ. Sci.* **9**, 3272 (2016).
100. G. Sahu *et al.*, *J. Mater. Chem. A* **2**, 10396 (2014).
101. A. K. Ivanov-Shitz *et al.*, *Crystallogr. Rep*. **46**, 864 (2001).
102. Y. M. Wang *et al.*, *J. Power Sources* **224**, 225 (2013).